Combined EGFR and ROCK Inhibition in Triple-negative Breast Cancer Leads to Cell Death Via Impaired Autophagic Flux

Authors

Stamatia Rontogianni, Sedef Iskit, Sander van Doorn, Daniel S. Peeper, and Maarten Altelaar

Correspondence

m.altelaar@uu.nl

In Brief

We aimed to identify the molecular mechanisms underlying the co-inhibition of EGFR and ROCK in triple-negative breast cancer (TNBC). We performed a deep (phospho)proteomic profiling between single and combination treatments and found autophagy as a mechanism implicated in the cells' response to combinatorial treatment. Particularly, we showed that EGFR inhibition alone induces autophagy, possibly as a cytoprotective mechanism for TNBC cells, however, on combinatorial treatment autophagic flux is impaired leading to an accumulation of autophagic vacuoles. We suggested the impaired autophagosome clearance as a likely cause of antitumor activity.

Graphical Abstract

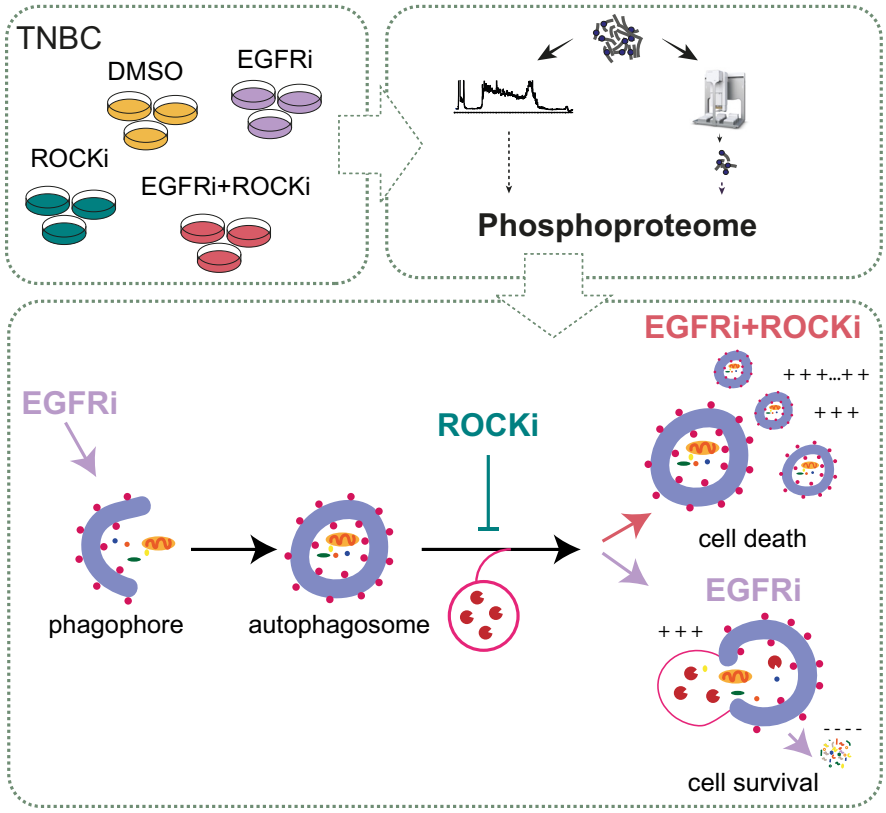

Highlights

- We used phosphoproteomics to reveal the underlying mechanisms of drug synergy on EGFR and ROCK co-inhibition in TNBC cells.
- EGFR inhibition alone induces autophagy activation in TNBC cells as a cytoprotective mechanism.
- Combinatorial treatment leads to impaired autophagic flux resulting in a strong accumulation of autophagic vacuoles.
- We hypothesize that ROCKi-induced cytoskeletal changes impair autophagosome clearance ultimately leading to cell death.

Rontogianni et al., 2020, Molecular & Cellular Proteomics *19*, 261–277
February 2020

https://doi.org/10.1074/mcp.RA119.001800

Combined EGFR and ROCK Inhibition in Triple-negative Breast Cancer Leads to Cell Death Via Impaired Autophagic Flux*[S]

Stamatia Rontogianni‡§, Sedef Iskit¶, Sander van Doorn‡§, Daniel S. Peeper¶, and Maarten Altelaar‡§‖**

Triple-negative breast cancer (TNBC) is an aggressive subtype of breast cancer with very limited therapeutic options. We have recently shown that the combined inhibition of EGFR and ROCK in TNBC cells results in cell death, however, the underlying mechanisms remain unclear. To investigate this, here we applied a mass spectrometry-based proteomic approach to identify proteins altered on single and combination treatments. Our proteomic data revealed autophagy as the major molecular mechanism implicated in the cells' response to combinatorial treatment. We here show that EGFR inhibition by gefitinib treatment alone induces autophagy, a cellular recycling process that acts as a cytoprotective response for TNBC cells. However, combined inhibition of EGFR and ROCK leads to autophagy blockade and accumulation of autophagic vacuoles. Our data show impaired autophagosome clearance as a likely cause of antitumor activity. We propose that the inhibition of the autophagic flux on combinatorial treatment is attributed to the major cytoskeletal changes induced on ROCK inhibition, given the essential role the cytoskeleton plays throughout the various steps of the autophagy process. ***Molecular & Cellular Proteomics 19: 261–277, 2020. DOI: 10.1074/mcp.RA119.001800.***

Triple-negative breast cancer (TNBC)[1], comprising 10–20% of all breast cancers, is an aggressive subtype of breast cancer, which is typically associated with poor prognosis. TNBC tumors are immunohistochemically defined by a lack of estrogen receptor (ER) and progesterone receptor (PR) expression as well as human epidermal growth factor receptor 2 (HER2) amplification and are therefore, insensitive to the established hormonal therapy and/or HER2 targeted treatment. Although it is possible to treat TNBC by surgery and systemic therapy, treatment-resistant recurrences are common (1). Despite extensive research, the absence of hormone receptors or a common genetic vulnerability has prevented the development of a clinically established targeted treatment against TNBC (2). Therefore, the development of new targeted therapies for patients with TNBC are urgently needed (3).

In TNBC, the epidermal growth factor receptor (EGFR) is frequently overexpressed, making it a potential therapeutic target. Currently, two types of EGFR inhibitors are being used in the clinic, small molecular tyrosine kinase inhibitors and monoclonal antibodies, which have already proven effective in other types of cancers, such as colorectal cancer. Unfortunately, no EGFR therapies are currently approved for TNBC because of low response rates, necessitating better markers for patient stratification (4) as well as the exploration of combination therapies (5, 6). In this light, two independent studies recently showed great synergistic antitumor activity when inhibitors of the RAF-MEK-ERK cascade were combined with autophagy inhibition in pancreatic and other RAS-driven cancers (7, 8).

Macroautophagy (hereafter referred to as autophagy) is a highly dynamic multi-step biological process of self-cannibalization that involves the degradation of damaged organelles, misfolded proteins and long-lived macromolecules in lysosomes. This process occurs under basal conditions for example, to degrade long-lived proteins, but is drastically elevated in cells under stress, such as starvation or hypoxia, as a protective mechanism, allowing cells to survive (9). Autophagy, which is characterized by the engulfment of cargo molecules by double-membrane vesicles, called autophagosomes, is an orchestrated process involving several steps. It starts with the formation and elongation of the phagophore, which enwraps and sequesters portions of the cytoplasm containing autophagic substrates, and then it expands through acquisition of lipids, and ultimately seals to generate a completed double membrane called autophagosome. Following closure, the autophagosome fuses with the lysosome

From the ‡Biomolecular Mass Spectrometry and Proteomics, Bijvoet Center for Biomolecular Research and Utrecht Institute for Pharmaceutical Sciences, Utrecht University, Padualaan 8, 3584 CH Utrecht, The Netherlands; §Netherlands Proteomics Center, Padualaan 8, 3584 CH Utrecht, The Netherlands; ¶Division of Molecular Oncology, The Netherlands Cancer Institute, 1066 CX Amsterdam, the Netherlands; ‖Mass Spectrometry and Proteomics Facility, The Netherlands Cancer Institute, 1066 CX Amsterdam, the Netherlands

Received October 29, 2019
Published, MCP Papers in Press, November 26, 2019, DOI 10.1074/mcp.RA119.001800

to form the autolysosome, where the sequestered cargo is degraded and recycled (10, 11).

In the context of cancer, the activation of autophagy is a double-edged sword. On the one hand, it functions primarily as a tumor suppressor mechanism, by clearing damaged organelles, maintaining cell homeostasis and protecting normal cell growth (12). Conversely, in established cancers, autophagy may become a key survival mechanism for tumor cells under a variety of stresses. For instance, evolving tumors develop regions of hypoxia and nutrient limitation, and under such harsh conditions, cancer cells adapt by inducing autophagy to protect themselves from cell death (13). Moreover, a growing body of evidence suggests that autophagy activation plays a cytoprotective role in cancer cells undergoing various anti-cancer treatments, resulting in poor treatment outcomes and the development of treatment resistance (14). Accordingly, preclinical studies have shown that genetic or pharmacological inhibition of cytoprotective autophagy can overcome therapy resistance and promote tumor regression (15–17).

We previously carried out *in vivo* and *in vitro* screens complemented with pharmacologic screens to identify drug combinations that effectively impair TNBC cell growth. We reported that combined inhibition of EGFR and ROCK induces cell cycle arrest in TNBC cells (18). However, the underlying mechanisms by which co-inhibition of EGFR and ROCK induces TNBC cell death remain unclear. Here, we set out to elucidate the synergistic effect of the combined treatment using mass spectrometry-based quantitative (phospho)proteomics. We employed a two-dimensional proteomic strategy by combining offline high-pH reversed phase fractionation with nanoLC-MS/MS for deep proteomic profiling in order to identify proteins and pathways altered on single and combination treatments. Interestingly, our data showed a significant increase in the expression levels of autophagy-related proteins on EGFRi-treatment, both at the proteome and phosphoproteome level, whereas combined treatment with EGFRi and ROCKi leads to impaired autophagy, resulting in increased cell death.

MATERIALS AND METHODS

Cell Culture and Inhibitors—MDA-MB-231 and Cal120 cells were cultured in Dulbecco's modified Eagle's medium (DMEM) supplemented with 10% fetal bovine serum (Sigma, Germany), 2 mM glutamine, 0.1 mg/ml penicillin and 0.1 ml/ml streptomycin (Gibco, Gaithersburg, MD). HCC1806 and Hs578T cells were maintained in RPMI supplemented with glutamine. All cells were maintained in a humidified incubator at 37 °C and 5% CO_2. All cell lines were obtained from ATCC and have been regularly tested for mycoplasma contamination. For the (phospho)proteomics and Western blotting experiments, drugs were added on the following day of seeding. Cells were treated with the inhibitors Gefitinib (EGFRi, MedChem) or GSK269962A (ROCKi, Axon, Groningen, The Netherlands) or their combination (EGFRi+ROCKi) using the following concentrations: Hs578T, Cal51, MDA-MB-231, Cal120 and HCC1806 cells were treated with 20 μM EGFRi. ROCKi concentrations were the following: for Hs578T 1.2 μM, for Cal51 12μM, for MDA-MB-231 4.8 μM, for HCC1806 2.4 μM and for Cal120 was 30 μM.

Sample Preparation for Mass Spectrometry—Cal51 and Hs578T cells were harvested in triplicates in cold PBS after a 2-day treatment with DMSO, EGFRi, ROCKi or combination (EGFRi+ROCKi). The cellular pellets were resuspended in lysis buffer containing 1% (w/v) sodium deoxycholate (SDC), 10 mM TCEP, 40 mM chloroacetamide, 100 mM Tris, pH 8.5, supplemented with 1 tablet of Complete mini EDTA-free mixture (Roche) and 1 tablet of PhosSTOP phosphatase inhibitor mixture (Roche, Indianapolis, IN) per 10 ml of lysis buffer, and subsequently lysed by boiling for 5 min at 95°C and sonication (Bioruptor, model ACD-200, Diagenode) for 15 min at level 5 (30 s ON, 30 s OFF). Cell debris was then removed by centrifugation at 20,000 × *g* for 15min at 4°C. Prior to in-solution digestion, the total protein concentration was quantified by Bradford assay (Bio-Rad, Hercules, CA). For label-free quantification, input amounts were normalized based on the total protein contents (50 μg of total protein lysate per sample). The lysate was diluted 1:10 with 50 mM ammonium bicarbonate for Lys-C and trypsin digestion. Protein digestion was performed overnight at 37 °C with Lys-C (Wako) at an enzyme/protein ratio 1:75 and trypsin (Sigma) at an enzyme/protein ration of 1:50. The digest was acidified by adding 4% formic acid (FA) to precipitate SDC and samples were subsequently desalted using Sep-Pak C18 cartridges (Waters Corporation, Etten-Leur, The Netherlands) and further submitted to phosphorylation enrichment or high pH fractionation for in-depth proteome analysis.

High-pH Reversed-phase Fractionation—50 μg of peptides of each sample were reconstituted in 10 mM ammonium hydroxide, pH 10 and loaded on a Gemini 3 μm C18 110 Å 100 × 1.0 mm column (Phenomenex) using an Agilent 1100 binary pump (Agilent Technologies, Santa Clara, CA). The peptides where concentrated on the column at 100 μl/min using 100% buffer A (10 mM Ammonium Hydroxide, pH 10) for 2 min after which the fractionation gradient initiated as follow: 5% solvent B (10 mM ammonium Hydroxide in 90% ACN, pH 10) to 30% B in 53 min, 70% B in 7 min and increased to 100% B in 3 min at a flow rate of 100 μl/min. In total 60 fractions of 1 min were collected using an Agilent 1260 infinity fraction collector, and were pooled into 5 fractions using the concatenation strategy as described (19). The pooled fractions were dried in a vacuum centrifuge and stored at −80°C until further analysis.

Mass Spectrometry Analysis—Nanoflow LC-MS/MS data were acquired on an Orbitrap Q Exactive Plus (Thermo Fisher, Bremen, Germany) coupled to an Agilent 1290 Infinity UHPLC (Ultra-High Pressure Liquid Chromatography) system (Agilent Technologies). Both the trap (Dr Maisch Reprosil C18, 3 μm, 2 cm × 100 μm) and the analytical (Agilent Poroshell EC-C18, 2.7 μm, 50 cm × 75 μm) columns were packed in-house. Peptides were trapped for 10 min at 5 μl/min in 100% solvent A (0.1 M acetic acid in water). Separation was performed at a column flow rate of ~300 nl/min (split flow from 0.2 ml/min) and the gradient was as follows: 13% up to 40% solvent B (0.1 M acetic acid in 80% acetonitrile) in 95 min, 40–100% in 3 min and finally 100% for 1 min. The mass spectrometer was programmed in the data-dependent acquisition mode. Full scan MS spectra from *m/z* 375–1,600 were acquired at a resolution of 35,000 with an automatic gain control (AGC) target value of 3e6. The 10 most intense precursor ions were selected for fragmentation using HCD. MS/MS spectra were obtained at a 17,500 resolution with an AGC target of 5e4. HCD fragmentation was performed at a normalized collision energy (NCE) of 25%.

[1] The abbreviations used are: TNBC, Triple-negative breast cancer; ER, estrogen receptor; PR, progesterone receptor; HER2, human epidermal growth factor receptor 2; EGFR, epidermal growth factor receptor.

Phosphopeptide Enrichment and MS Analysis—Phosphopeptide enrichment was performed using a combination of Fe(III)-IMAC cartridges and an automated setup, the AssayMAP Bravo Platform (Agilent Technologies) as described previously (20). Briefly, Fe(III)-NTA cartridges were primed with 250 μl of 0.1% TFA in ACN and equilibrated with 250 μl of loading buffer (80% ACN/0.1% TFA). Per sample, 50 μg of digested peptides were dissolved in 200 μl of loading buffer and loaded onto the cartridge. The columns were washed with 250 μl of loading buffer, and the phosphorylated peptides were eluted with 25 μl of 1% ammonia directly into 25 μl of 10% formic acid. Subsequently, the samples were dried down in a vacuum centrifuge. Next, phosphopeptides were reconstituted in loading buffer containing 10% formic acid and analyzed by nanoLC-MS/MS on a Q Exactive HF (ThermoFisher Scientific) coupled to an Agilent 1290 Infinity System (Agilent Technologies). As previously described, eluted phosphopeptides were delivered to a trap column (100 μm i.d. $\times$ 2 cm, packed with 3 μm C18 resin, Reprosil PUR AQ, Dr. Maisch) at a flow rate of 5 μl/minute in 100% loading solvent A (0.1% FA, in HPLC grade water). After 10 min of loading and washing, peptides were transferred to an analytical column (75 μm i.d. $\times$ 50 cm, packed with 2.7 μm Poroshell 120 EC C18, Agilent Technologies) and eluted at room temperature using an 95 min with an LC gradient from 8% to 32% solvent B (0.1% FA, 80% ACN). The Q Exactive HF was operated in data-dependent acquisition mode using the following settings: full-scan automatic gain control (AGC) target 3e6 at 60,000 resolution; scan range 375–1600 *m/z*; Orbitrap full-scan maximum injection time 20 ms; MS2 scan AGC target 1e5 at 30,000 resolution; maximum injection time 50 ms; normalized collision energy 27; dynamic exclusion time 16s; isolation window 1.4 *m/z*; 12 MS2 scans per full scan.

Data Processing—Raw MS files were processed with MaxQuant (version 1.6.2.3) (21). The Andromeda search engine (22) was used to search the MS/MS data against the forward and reverse Human Uniprot database (20,386 entries, August 2018). Trypsin/P was specified as enzyme allowing up to two missed cleavages. Cysteine carbamidomethylation was set as a fixed modification, whereas methionine oxidation and protein N-term acetylation were set as variable modifications. For the phosphoproteome analysis, serine, threonine and tyrosine were selected as variable modification. A false discovery rate (FDR) of 1% was applied at the level of proteins, peptides and modifications. The minimum peptide length was set to 7 residues and an additional peptide score cut-off of 40 was set for modified peptides. The mass tolerance was set to 4.5 ppm for the precursor ions and 20 ppm for the fragment ions. Label free quantification (LFQ) was performed using the MaxLFQ algorithm (23) integrated into MaxQuant with the following parameters: LFQ minimum ratio count was set to 2, the Fast LFQ option was enabled, LFQ minimum number of neighbors was set to 3, and the LFQ average number of neighbors to 6. The "match between runs" feature was enabled with a match time window of 0.7 min and an alignment time window of 20 min.

Experimental Design, Data Analysis and Statistical Rationale—For each experiment, Hs578T and Cal51 cells were treated either with DMSO (control), gefitinib (EGFRi), GSK269962A (ROCKi) or with their combination treatment (EGFRi+ROCKi) ($n = 4$). To increase the statistical power, experiments were performed in three biological replicates, starting from separate cultures, while no technical replicates were measured. To increase proteomic coverage, five high pH fractions per condition were collected and measured for proteomics ($n = 60$) analysis. Phosphoproteome analysis ($n = 12$) was performed only in the Hs578T cells. Pearson correlation coefficients between biological replicates exceeded 0.9, and thus no sample was excluded from the Hs578T cells. On the contrary, in the Cal51 treated cells, one of the three biological replicates from the EGFRi-treated condition was an outlier as evident by the Pearson's correlation and the PCA analysis and was therefore excluded from the analysis. All data were analyzed using the Perseus software (24). LFQ intensities extracted by MaxQuant were Log_2 transformed. The samples were grouped in triplicates (DMSO, EGFRi, ROCKi and EGFRi+ROCKi) and identifications were subsequently filtered for proteins having at least 2 valid values in at least one treatment group. Missing values were imputed on a basis of normal distribution with a downshift of 1.8 SDs and a width of 0.3 SDs, enabling statistical analysis. Only class I phosphorylation sites (localization probability $p > 0.75$) were used in subsequent phosphoproteome analyses. For hierarchical clustering, logarithmized LFQ intensities were first z-scored and subsequently clustered using Euclidean as a distance for column and row clustering. Principal component analysis (PCA) was performed using Perseus' built-in tool. Differences in the protein levels between the different treated samples were calculated using an ANOVA test followed by a Benjamini-Hochberg multiple testing correction with a 5% FDR. Pair-wise comparisons were performed using student's *t* test. As significantly changing proteins we considered those with a *p* value <0.05 and a greater than 1.5-fold-change for the LFQ intensities between the treated conditions. Gene ontology (GO) analyses were performed with Database for Annotation, Visualization and Integrated Discovery (DAVID) v6.8 (25, 26). Protein-protein interaction network analysis was performed using the Cytoscape StringApp (27, 28). Significant enrichment of kinase linear motifs was performed using Fisher exact test within Perseus with an FDR of 0.05.

Western Blot Analysis—Cells were harvested in ice by scraping in ice cold 1$\times$ PBS and the pellets were lysed in RIPA buffer (50 mM TRIS pH 8.0, 150 mM NaCl, 1% Nonidet P40, 0.5% sodium deoxycholate, 0.1% SDS, complete protease inhibitor mixture (Roche), and phosphatase inhibitors 10 mM NaF, 1 mM Na_3VO_4, 1 mM sodium pyrophosphate, 10 mM beta-glycerophosphate). After sonication and centrifugation, the protein concentrations were determined using the Bio-Rad protein assay (Bio-Rad). Equal protein amounts were loaded on 4–12% Bis-Tris polyacrylamide-SDS gels (NuPAGE) and transferred on to nitrocellulose membranes (Amersham Biosciences, Amersham, UK). Membranes were blocked in 4% skimmed milk powder dissolved in 0.2% Tween-containing 1$\times$ PBS and incubated with primary antibodies followed by secondary antibodies (Invitrogen, Carlsbad, CA). Primary antibodies used were LC3 (5F10, Nanotools, Germany), p62 (610832, BD Biosciences, Vianen, The Netherlands), $AMPK_{Thr172}$ (40H9, Cell Signaling, Leiden, The Netherlands), rpS6 (5G10, Cell Signaling), $rpS6_{Ser235/236}$ (Cell Signaling), Hsp90 (sc-7947, Santa Cruz, Heidelberg, Germany), Actin (AC-74, Sigma).

Autophagy Detection and Quantification by Cyto-ID Staining—Autophagy was measured using the CYTO-ID Autophagy Detection Kit (Enzo Life Sciences, Lausen, Switserland), according to the manufacturer's detailed instructions provided. Briefly, 6×10^3 Hs578T cells were seeded in 96-well plates overnight and then treated with the respective drug treatments (DMSO, EGFRi, ROCKi, EGFRi+ROCKi) on the following day. After 20 h of treatment, cells were stained with the Cyto-ID dye and the green fluorescent autophagic vacuoles were subsequently visualized using the IncuCyte System (Essen Bioscience, Garden City, UK). Acquired images were analyzed using the IncuCyte software and green fluorescent objects were counted enabling the "Top-Hat" feature, which estimates and subtracts local background from the image. To monitor autophagic flux, cells were analyzed by confocal microscopy. Approximately, 25×10^3 cells were seeded on glass bottom imagining dishes (μ-Dish 8 well, Ibidi) and after overnight incubation with the single and combination treatments, addition of 40 μM chloroquine (Enzo Life Sciences) followed. Subsequently, cells were stained with the Cyto-ID Green Detection Reagent and the Hoechst 33342 Nuclear Stain (Enzo Life Sciences), fixed for 15 min with 4% paraformaldehyde (PFA) and subsequently analyzed by a confocal laser scanning microscope Carl Zeiss LSM

700 with a 40x oil-immersion objective lens. Green puncta in confocal images were quantified by ImageJ in combination with the ComDet (pluginhttps://github.com/ekatrukha/ComDet/wiki). Significant differences between the CLQ treated and untreated samples were analyzed using student's *t* test (two-tailed) to compare the two groups, with a p value <0.05 to be considered significant.

RESULTS

Proteomic Profiling of TNBC Cells on Single and Combination Treatments—To gain understanding of the mechanisms underlying the synergistic effect of the combined inhibition of EGFR and ROCK in triple-negative breast cancer cells we performed a mass spectrometry-based proteomics analysis. As a model system for our study, we selected the triple-negative breast cancer cell line Hs578T, to identify proteomic differences in signaling on treatment with either of the two single inhibitors and their combination treatment. Thus, Hs578T cells were treated either with DMSO (control), gefitinib (EGFRi), GSK269962A (ROCKi) or with their combination treatment (EGFRi+ROCKi). Consistent with our previous findings (18), EGFRi+ROCKi inhibition significantly impaired the TNBC cell growth compared with the EGFRi and ROCKi alone (Fig. 1*A*). To gain insight into the global signaling changes occurring across the different treatments, we employed a label-free quantitative (phospho)proteomics approach. Briefly, cells were treated for 48h, lysed and subsequently the protein extracts were in-solution digested by LysC/trypsin. To obtain a deep proteome coverage, we generated five fractions by off-line high-pH reverse phase chromatography (HpH) (19). In parallel, for the phosphoproteomics analysis, an automated phosphopeptide enrichment step was performed using Fe(III)-IMAC cartridges on an AssayMAP Bravo platform as has been previously described (20). All samples were analyzed by nanoLC-MS/MS coupled to a quadrupole Orbitrap high resolution mass spectrometer (Q Exactive Plus) followed by data analysis in MaxQuant. In total, we identified 7,169 proteins and 22,758 phosphosites with a localization probability >0.75. However, for further data analysis we only considered a stringently filtered data set of 5,783 proteins and 7,387 phosphosites, respectively, with quantitative values in at least two out of three biological replicates ("quantified"; Fig. 1*B*, Supplemental Data set S1 and S2).

For an overall assessment of the effect of the four different treatment conditions on the global proteome profiles we employed principal component analysis (PCA). As can be seen in Fig. 1*C*, all biological replicates of each condition clustered together, whereas principal component 1 (PC1) and principal component 2 (PC2) revealed a clear partition between the different treatments. PC1 clearly separated the DMSO and EGFRi treated samples from the ROCKi and EGFRi+ROCKi, whereas PC2 showed a segregation of the EGFRi and EGFRi+ROCKi from the rest and account for 33.1% and 21.2% of the variability, respectively. The trend observed by PCA was confirmed by the Pearson correlation coefficients of the proteome data (Fig. 1*D*). The Pearson correlations between the biological replicates and between the different treatments was >0.96 and >0.91, respectively.

Comparative Analysis Between Different Treatment Conditions Revealed An Additive Effect of EGFR and ROCK Inhibition on Combination Treatment—Next, to address the statistical differences between the different drug treatments and obtain a view of potential functional proteomic changes, we performed an ANOVA test (FDR $< 5\%$), which identified 995 significantly changing proteins between any of the four conditions (Fig. 2). Hierarchical clustering of these proteins revealed again a clear separation between the single inhibitor treatments (EGFRi and ROCKi) and a partial overlap with either of the two on combination treatment of the Hs578T cells. In particular, the heatmap showed segregation of the ANOVA significant proteins into three main clusters; one, which was specific to proteins downregulated in the EGFRi+ROCKi treatment (cluster A) and two that included upregulated proteins that were common between the EGFRi+ROCKi treatment with the EGFRi (cluster B) and the ROCKi (cluster C) treatments, respectively (Fig. 2). Gene ontology (GO) analysis of the proteins in cluster A revealed that EGFRi+ROCKi treatment resulted in downregulation of nuclear and adhesion proteins, and subsequently downregulation of biological processes including chromatin remodeling, mRNA processing and cell adhesion. Enrichment analysis of the proteins in cluster B showed that proteins upregulated in the EGFRi and EGFRi+ROCKi treatments were involved in cellular processes including cholesterol biosynthesis, oxidation-reduction and autophagy, whereas proteins in cluster C (high expression in ROCKi and EGFRi+ROCKi) revealed strong enrichment of the terms cell adhesion, regulation of mRNA stability and intracellular protein transport. Interestingly, on ROCKi and EGFRi+ROCKi treatments we observed an upregulation of the proteasome complex, indicating the implication of another degradative pathway (together with autophagy) in the EGFRi+ROCKi treated cells.

In addition, comparative analysis performed on the phosphoproteome data revealed 1,052 phosphosites to be differentially regulated (ANOVA, p value < 0.05) on the different treatments. In agreement with the proteome data, unsupervised hierarchical clustering of the regulated phosphosites and subsequent gene ontology (GO) analysis of the respective clusters showed a large effect on processes related to transcription, cell-cell adhesion and cytoskeleton organization (both actin and microtubule cytoskeleton) on EGFRi+ROCKi treatment (supplemental Fig. S1*A*). Interestingly, our phosphoproteome data revealed a cluster of 445 phosphosites (cluster D; supplemental Fig. S1), which were found to be specifically downregulated only on combination treatment. To decipher how signaling pathways are modulated by EGFRi+ROCKi treatment, we investigated which phosphorylation motifs are enriched in this cluster of downregulated phosphosites (supplemental Fig. S1*B* and supplemental Table S1), (Fisher exact test, FDR<0.05). Kinase-substrate motif enrichment

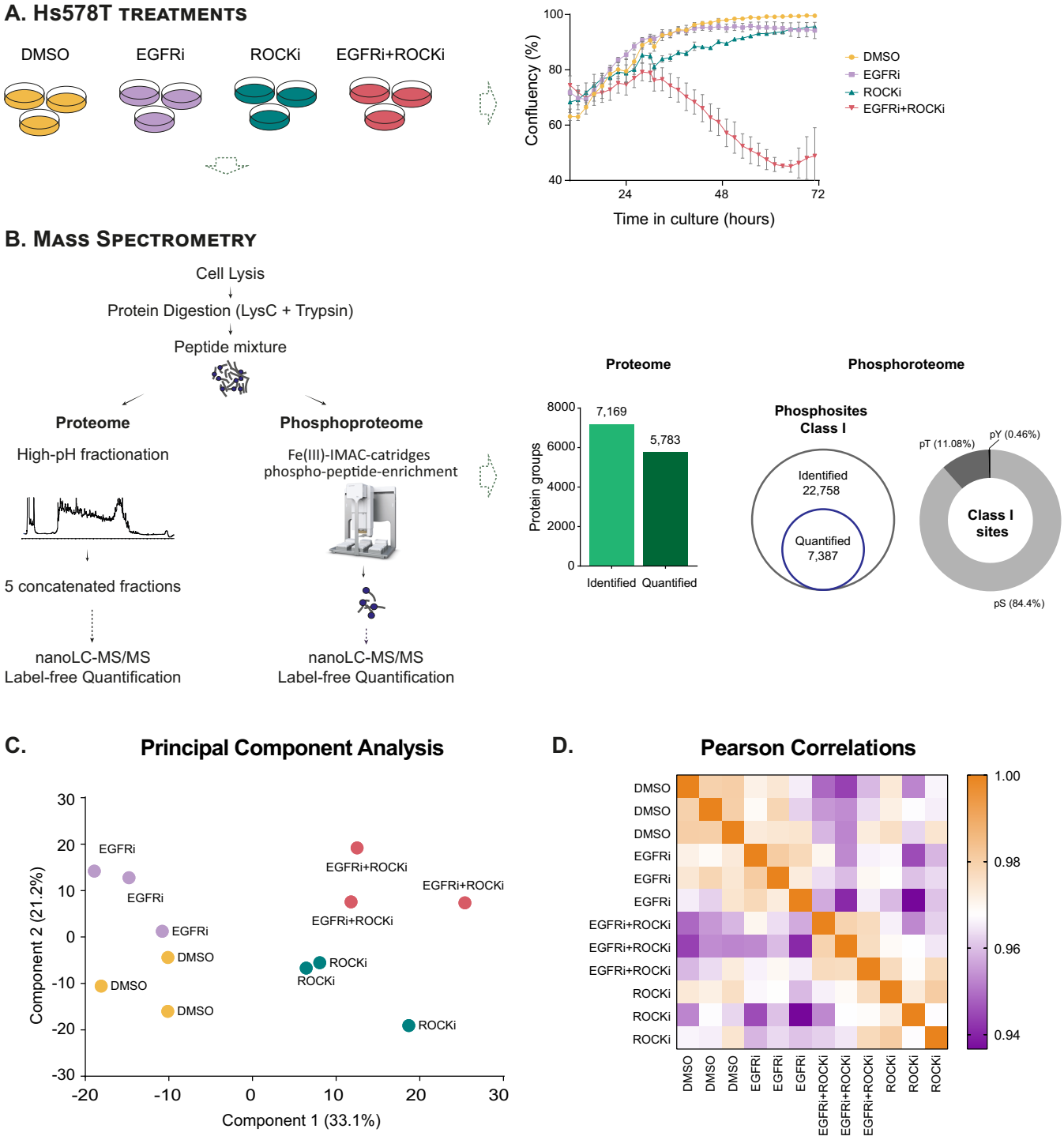

FIG. 1. **Experimental design and overview of the proteome data.** *A*, Hs578T cells were treated respectively with DMSO, EGFRi (gefitinib), ROCKi (GSK269962A) or EGFRi+ROCKi combination treatments. Cell viability measured up to 72-h (3 days) treatments. *B*, Phospho(proteomics) workflow. After cell lysis, proteins were digested using LyC/trypsin. For in-depth proteome analysis, peptides were fractionated by high-pH reversed-phase chromatography and concatenated into 5 fractions prior to nanoLC-MS/MS analysis. Phosphopeptide enrichment was performed using an automated Fe(III)-IMAC workflow on the Bravo AssayMAP Platform. Bar plot of the total number of identified and quantified proteins. Total number of class I phosphosites identified and quantified. Distribution of Ser/Thr/Tyr phosphosites identified. *C* and *D*, Principal component analysis (PCA) and heatmap of the Pearson correlations coefficients based on their global proteomic expression profiles. Both PCA analysis and Pearson correlation coefficients showed clustering of replicates and a clear separation between the different treatment conditions.

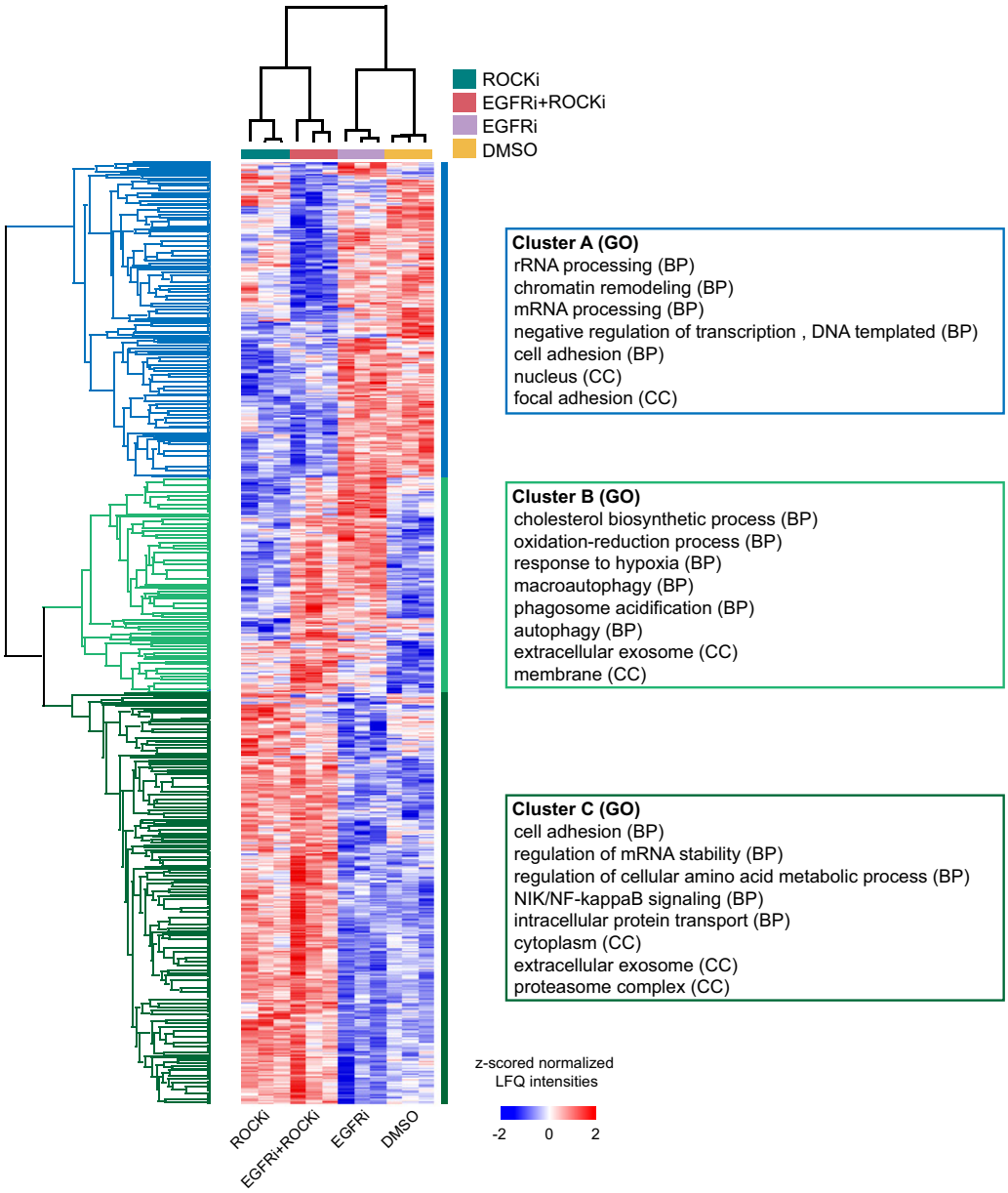

FIG. 2. **Proteins differentially expressed across different treatments.** Heatmap showing relative protein expression values (z-scored and Log_2-transformed LFQ protein intensities) of the differentially expressed proteins (ANOVA, FDR < 0.05) between the different samples after unsupervised hierarchical clustering. On the right, gene ontology analysis of proteins significantly downregulated (Cluster A) and upregulated (Clusters B and C) in EGFRi+ROCKi treatment.

analysis showed the most significant enrichment for substrate motifs of the PKA and PKC kinases, which belong to the same AGC family of serine-threonine kinases as ROCK1. The substrate motifs for PKA and PKC are better defined and have been shown to overlap with ROCK (29). Other motifs belong to kinases downstream of EGFR, regulating key pro-survival signaling and cell cycle-related pathways such as MAPK, PAK2 and CDKs (supplemental Fig. S1*B*).

Differentially Expressed Autophagy-related Proteins in EGFRi, ROCKi and EGFRi+ROCKi Treatments—The quantitative comparison between the different treatment conditions revealed a cluster of proteins involved in the process of autophagy to be significantly upregulated on single EGFR and dual EGFR and ROCK inhibition, indicating that autophagy might play a role in the TNBC cells' response to therapy. Therefore, to further mine our quantitative data and provide insights into the molecular changes induced on each treatment condition, we performed pairwise comparisons of each treatment condition (EGFRi-, ROCKi- and EGFRi+ROCKi-treated cells) to its untreated control (DMSO-treated cells) and focused on the differential regulation of autophagy-related proteins.

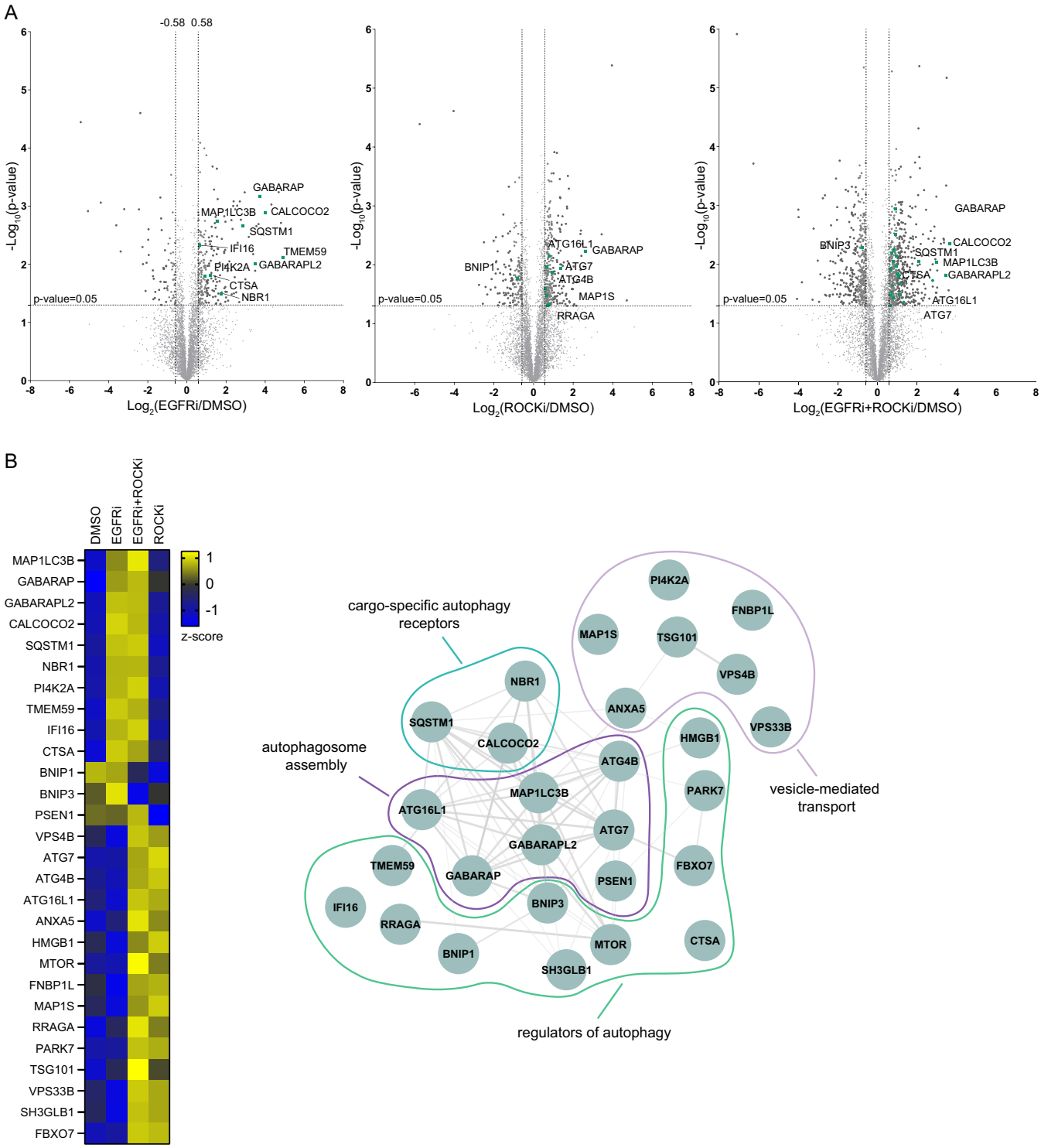

FIG. 3. **Autophagy-related proteins differentially expressed in EGFRi, ROCKi and EGFRi+ROCKi treatments.** *A*, Volcano plots of the *p* values *versus* the Log_2 protein abundance differences between different treatment conditions; significantly enriched autophagy-related proteins are highlighted in green. *B*, Heatmap showing z-scored and Log_2-transfromed LFQ protein intensities of the autophagy-related proteins across the different treatments and their protein-protein interaction network.

As shown in Fig. 3, gefitinib treatment (EGFRi) compared with the DMSO-treated cells resulted in upregulation of known autophagic markers. Among them, we detected the autophagy-related protein LC3B (MAP1LC3B), which is used as a phagophore or autophagosome marker, and the GABARAP and GABARAPL2 proteins, which are involved in

the later stages of autophagosome formation, in particular the phagophore elongation and closure (30). Moreover, the cargo-specific autophagy receptors CALCOCO2, SQSTM1/p62 and its paralogue NBR1, the autophagy regulator TMEM59 and the lipid kinase PI4K2A, which plays a role in the autophagosome-lysosome fusion (31), were also upregulated in response to gefitinib treatment.

When we compared the proteomes of cells treated with ROCKi alone to the untreated control and looked for changes in the expression levels of known autophagy markers, we identified several proteins to be upregulated on ROCK inhibition. We identified the GABARAP receptor together with the autophagy-related (ATG) genes ATG7, ATG16L1 and ATG4B, which participate in the formation of phagophores and the initiation of autophagy (32). Moreover, proteins with known roles in the regulation of autophagy such as the GTPase RRAGA, which activates autophagy in response to amino acids (33) and the microtubule-associated protein MAP1S, which is required for autophagosome trafficking along microtubular tracks (34) showed increased expression on ROCKi treatment.

Finally, consistent with the ANOVA significantly changing proteins on combination treatment, proteome expression changes in the EGFRi+ROCKi treated cells compared with the control cells (DMSO) revealed an accumulation of many autophagy-related proteins showing an enhanced and partly combinatorial effect of the regulation changes in the respective single treatments. An overview of the differentially regulated autophagy-associated proteins and their abundances across the different treatments is presented in the heatmap in Fig. 3*B*, along with their protein-protein interaction network.

These findings further indicated the autophagy process as a potential pathway induced by the cells on combination treatment, which might eventually cause cell death.

EGFRi+ROCKi Treatment Induces Autophagy in TNBC Cells—To exclude that autophagy induction is a cell line-specific (Hs578T cells) response to the combinatorial treatment, and to determine whether it can be considered a general process in the response of TNBC cells, we decided to analyze the proteomic changes on EGFRi+ROCKi treatment in another TNBC cell line. To this end, we chose the Cal51 cell line, whose sensitivity to EGFRi+ROCKi treatment has been previously reported as well (18). Following the same experimental workflow as the Hs578T cells, the proteomes of Cal51 cells treated for 48 h with DMSO, EGFRi, ROCKi and EGFRi+ROCKi were compared by label-free quantitation (supplemental Data set S2). Like the Hs578T cells, PCA analysis showed co-clustering of all the biological replicates of each treatment condition, except for one EGFRi-treated sample, which was an outlier and was therefore excluded from further analysis. In addition, the EGFRi- and DMSO-treated samples clustered close together, whereas ROCKi treated samples clustered with the EGFRi+ROCKi treated samples. These proteome similarities were also reflected in the Pearson correlations (supplemental Fig. S2).

Furthermore, unsupervised hierarchical clustering of the 738 proteins, which were differentially expressed across the different treatment conditions (ANOVA, FDR$<$0.05) showed an enrichment in proteins involved in similar biological processes as those found on the Hs578T cells. For instance, treatment of Cal51 cells with ROCKi and EGFRi+ROCKi resulted in downregulation of nuclear proteins involved in transcription, rRNA processing and cell cycle. Additionally, treatment of Cal51 cells with single EGFR and combined EGFR+ROCK inhibitors showed upregulation of proteins involved in autophagy, whereas ROCKi and EGFRi+ROCKi treatments resulted in upregulation of cell-cell adhesion, protein transport and an increase in the expression levels of protein of the proteasome complex (supplemental Fig. S3*A*). Moreover, the specific autophagy-related proteins and their differential regulation across each treatment condition are highlighted in the respective volcano plots (supplemental Fig. S3*B*). Again, an additive effect on the expression of autophagy related proteins is observed in the proteome changes induced on combination treatment.

We next set out to validate our mass spectrometry data and the induction of autophagy by Western blot analyses in a panel of TNBC cell lines, including MDA-MB-231, the cell line in which the synergistic effect of EGFR and ROCK inhibition combination was initially shown (18). Following the induction of autophagy, the microtubule-associated protein LC3, MAP1LC3 (MAP1LC3-I) is converted to membrane bound phosphatidylethanolamine (PE)-conjugated MAP1LC3 (MAP1LC3-II), and the expression of MAP1LC3-II is frequently used as a phagophore or autophagosome marker (35). We therefore evaluated the expression levels of this protein as well as those of p62 (SQSTM1), which as mentioned previously is a known autophagy receptor that links ubiquitinated proteins to MAP1LC3. As shown in Fig. 4*A*, in MDA-MB-231 cells, EGFR inhibition compared with DMSO treatment resulted in an increase in the protein levels of the MAP1LC3-II and the p62 (SQSTM1) proteins, indicating autophagy induction. When cells were treated with EGFRi+ROCKi the protein levels of LC3-II and p62 remained high, whereas ROCKi treatment alone did not have any influence on autophagy. Interestingly, although combined inhibition of EGFR and ROCK led to increased AMPK phosphorylation, which is another indication of autophagy induction, p-AMPK was not detected in cells treated with EGFRi alone. Finally, in MDA-MB-231 cells, we observed a steep decrease in phosphorylated rpS6 levels on ROCK inhibition whereas, rpS6 phosphorylation declined even further in the case of combined EGFRi+ROCKi treatment, which is indicative of an inactive state of the mTOR pathway (36) and which has been previously associated with cell growth inhibition and cell cycle arrest induction (37). The drug-induced changes in the levels of LC3-II protein and the phosphorylation status of rpS6 were

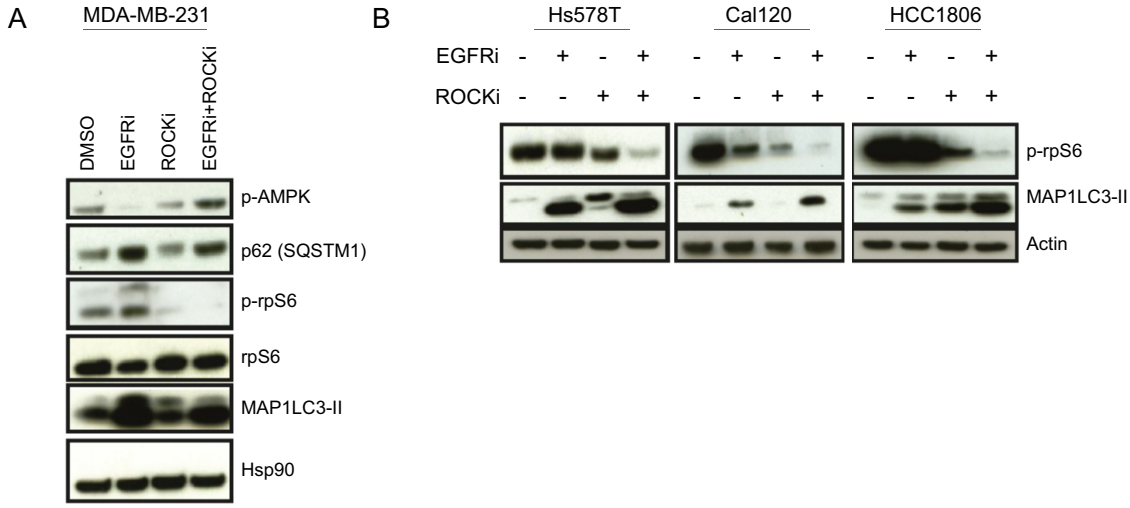

FIG. 4. **Autophagy induction in TNBC cells.** *A*, Western blot analyses to evaluate the protein expression levels of known autophagy markers and rpS6 phosphorylation in DMSO, EGFRi, ROCKi and EGFRi+ROCKi treated MDA-MB-231 cells. Hsp90 is used as a loading control. *B*, Western blot analyses of LC3-II (MAP1LC3-II) and phosphorylated rpS6 levels in Hs578T, Cal120 and HCC1806 cells. Actin is used as a loading control.

reproducible in the triple-negative cell lines Hs578T, Cal120 and HCC1806 (Fig. 4*B*).

EGFRi+ROCKi Treatment Impairs Autophagic Flux—The results presented thus far provide compelling evidence that combined inhibition of EGFR and ROCK triggers autophagy induction in triple-negative breast cancer cells, however, how autophagy induction leads to cell death remains unclear. Therefore, in a next step we decided to monitor autophagic activity in live cells treated with DMSO, EGFRi, ROCKi and EGFRi+ROCKi, respectively.

To do so, treated Hs578T cells were stained with the Cyto-ID autophagy green dye, which specifically labels autophagic vacuoles, and were visualized using live cell imaging in the IncuCyte System (supplemental Fig. S4). The dye enables clear detection and quantification of autophagic and pre-autophagic vacuoles that directly correlate with induction of autophagy (38). The control group (DMSO) exhibited faint Cyto-ID green fluorescence whereas EGFR inhibition by gefitinib treatment resulted in the appearance of green autophagic vacuoles in the cells. By contrast, no significant autophagy was identified in the ROCKi-treated cells. Moreover, in the combination treatment, inhibition of ROCK activity did not abolish the autophagy induction mediated by gefitinib treatment, but instead resulted in an increased number of stained autophagic vacuoles compared with the EGFRi-treated cells. This accumulation of autophagic vacuoles in the EGFRi+ROCKi-treated cells can either be a result of increased stimulation of autophagy resulting in rapid formation of autophagic vacuoles or because of inefficient autophagosome turnover and clearance caused by impaired autophagosome-lysosome fusion. Thus, in order to distinguish between these two possibilities, we assessed the autophagic flux by monitoring the accumulation of autophagic compartments induced by chloroquine (CLQ), a lysosome inhibitor that blocks the fusion of autophagosomes and lysosomes (39). As shown in Fig. 5, combined treatment of EGFRi+CLQ resulted in a significant increase in the number of autophagic vacuoles compared with EGFRi alone, because of impaired autophagic flux. The addition of CLQ to EGFRi treatment raised the number of observed autophagic vacuoles to a similar level as observed for our EGFRi+ROCKi combination treatment. On the other hand, co-administration of EGFRi+ROCKi with CLQ did not cause a significant increase in the autophagic vacuoles formation compared with the EGFRi+ROCKi treatment alone. These results indicate that EGFRi+ROCKi does not stimulate autophagic flux in Hs578T cells, beyond to that seen by single inhibition, and that the increase in autophagic vacuoles is most likely caused by impaired autophagosome clearance instead of increased vacuole formation.

Next, to demonstrate that the inhibition of EGFRi-induced autophagy results in cell death, we monitored cell growth of DMSO-, EGFRi-, ROCKi- and EGFRi+ROCKi-treated Hs578T cells with or without chloroquine treatment (CLQ; autophagy inhibitor) for ~7 h. As expected, the pharmacological inhibition of autophagy with 40 μM CLQ resulted in impaired cell growth and ultimately cell death in the EGFRi and (even stronger) in EGFRi+ROCKi cells compared with the untreated (no CLQ) conditions (supplemental Fig. S5). Conversely, addition of CLQ in the DMSO and ROCKi treated cells did not have any impact on the cell growth.

Taken together, these findings indicate that cell death on EGFRi+ROCKi treatment occurred because of autophagy blockade and impairment of the EGFRi-induced autophagic flux and ROCK activity is essential for an efficient autophagy process.

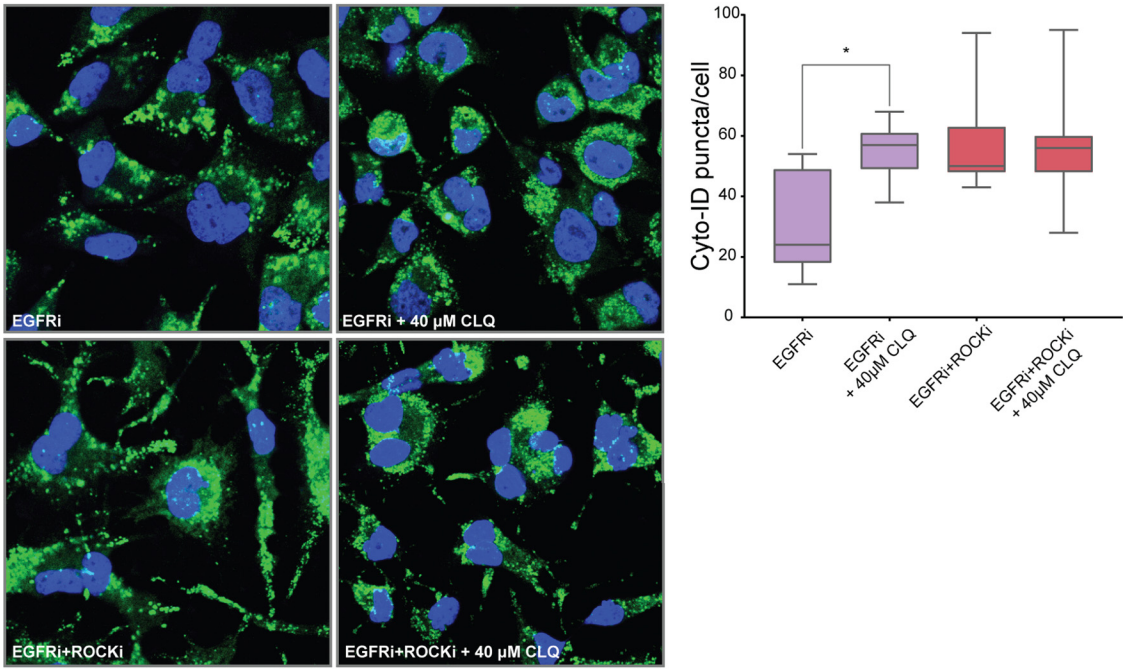

FIG. 5. **Autophagic flux in EGFRi and EGFRi+ROCKi-treated cells.** EGFRi- and EGFRi+ROCKi-treated Hs578T cells, were incubated for 2 h in the absence or presence of 40 μM chloroquine (CLQ) and subsequently stained with the Cyto-ID dye (green). Nuclei were counter-stained with Hoechst 33342 dye (blue). Images were obtained by confocal microscopy and autophagic vacuoles were counted to assess autophagic flux per treatment condition. The graph on the right shows the average of Cyto-ID puncta per cell (n = 15,*p value <0.01 from two-sided, unpaired t test).

ROCKi-associated Cytoskeletal Changes Affect Autophagy—As inhibition of ROCK activity led to impaired autophagy, we next set out to investigate the mechanisms underlying this effect. As revealed by the gene ontology enrichment analysis of the ANOVA significant proteins and phosphosites (Fig. 2 and supplemental Fig. S1), ROCK inhibition had a substantial effect on the expression levels of several cytoskeletal and focal adhesion proteins. This finding is consistent with the involvement of ROCK in the regulation of cell shape and movement (40) and was also evident from the major morphological changes that occurred in the cells on ROCKi and EGFRi+ROCKi treatment, where cells became flattened and acquired neuron-like long extensions. Recent evidence indicates an important role of actin cytoskeleton dynamics together with myosin motor proteins in the various steps of the autophagy process, ranging from the early stages of phagophore formation and expansion, to autophagosome trafficking and fusion with the lysosome (41, 42). In line with these findings, we observed marked changes in the expression levels of proteins involved in focal adhesion and the regulation of the actin and microtubule cytoskeleton, which were down and upregulated, respectively (Fig. 6), on combination treatment.

Actin filament networks have been previously suggested to have a scaffolding role in generating the shape of the phagophore with the recruitment of the Arp2/3 complex that is known to promote actin branching and polymerization inside the expanding phagophore (43–45). Interestingly, in our data we observed upregulation of the actin related proteins ACTR2, ACTR3 and ARPC1B, in the EGFRi+ROCKi treated cells, which are core subunits of the Arp2/3 complex. On the other hand, the actins, alpha-actin-2 (ACTA2) and gamma-actin (ACTG1), together with several actin binding proteins such as the tropomyosin alpha-1 chain (TPM1), the drebrin (DBN1), the actin filament associated protein 1 (AFAP), the coronin-1C (CORO1C), nexilin (NEXN), which are essential in stabilizing cytoskeleton actin filaments, were downregulated. Furthermore, among the downregulated proteins on EGFRi+ROCKi treatment, we detected proteins involved in actomyosin-based motility such as the proteins anillin (ANLN), the myosin light chain kinase (MYLK) and the myosin phosphatase Rho interacting protein (MPRIP) that regulate actin-myosin interactions as well as proteins playing a role in actin cytoskeleton and microtubule stabilization such as cytospin-A (SPECC1L) and the formin-binding protein 1-like (FNBP1L).

It has been shown that autophagosome movement in the cytoplasm is dependent on microtubules (46). Once the autophagosomes are formed, they move along microtubular tracks toward the microtubule-organizing center where lysosomes are enriched (47). Here, on combination treatment, we found several tubulins and tubulin-associated proteins to be upregulated, including the microtubule-associated proteins MAP1S and MAP1B, which interact with LC3-I and LC3-II and recruit them to stable microtubules (34). However, in contrast to the proteome data, our phosphoproteome data showed a

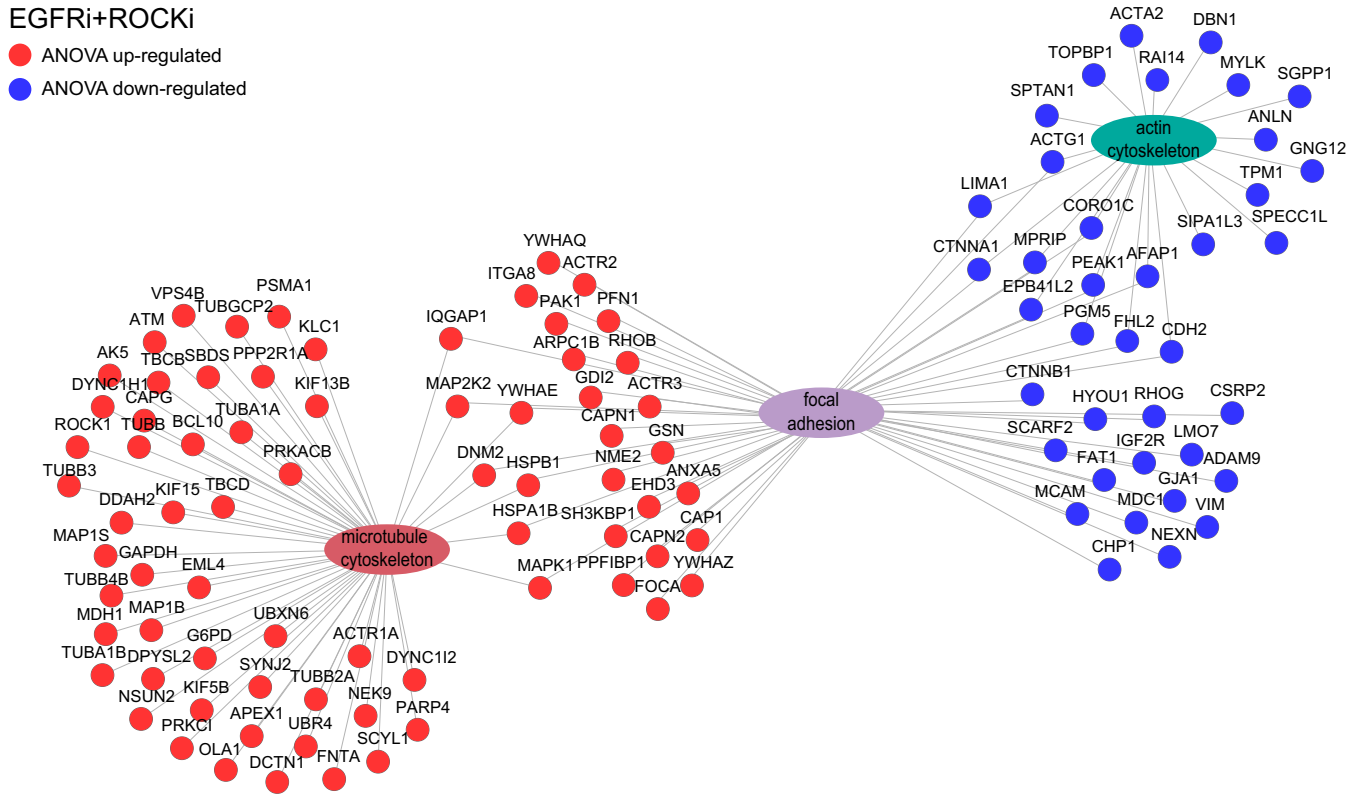

FIG. 6. **Overview of the differentially expressed cytoskeleton-related proteins on ROCK activity inhibition.** Functional enrichment network of the ANOVA significant up (red) and downregulated (blue) cytoskeleton-related proteins in the combination treatment using the *ToppCluster* tool (FDR correction, p value < 0.05) (68).

significant downregulation on the phosphorylation status of several proteins involved in the microtubule cytoskeleton organization. Within the identified downregulated phosphosites, we found multiple sites of the microtubule associated proteins MAP1B (S891, S1881, S992, S995, S1339, S832, S831, S1144, T1932) and MAP4 (S1151, S941, S507, S510). Although the exact functionality of the different phosphosites has not been yet investigated, several lines of evidence suggest that the binding of MAPs to microtubules is regulated by phosphorylation (48). Moreover, within the cluster of the EGFRi+ROCKi significantly changing phosphosites (cluster D, supplemental Fig. S1), the majority of the detected downregulated phosphosites belonged to proteins with key roles in cytoskeleton regulation. A network of the identified hypo-phosphorylated proteins on EGFR and ROCK inhibition, highly enriched in cytoskeleton-related terms is shown in the supplemental Fig. S6*A*.

Next, to further investigate the changes in autophagy regulation and find a potential link to the ROCKi-induced cytoskeletal changes, we focused our analysis on the autophagy-related proteins whose phosphorylation status was significantly altered between the different treatments (ANOVA, FDR<0.05). Compared with the proteome data, where the abundance levels of the autophagy-related proteins followed the same trend between the EGFRi and EGFRi+ROCKi treatments, at the phosphoproteome level for many proteins we observed an opposite trend (supplemental Fig. S6*B*). Interestingly, among the proteins with differentially regulated phosphosites, we found the myosin MYO1C (S864), the SNARE protein STX12 (S139 and S142) and the actin binding SYNPO2 (S930, S902, S226, S777) to be hypo-phosphorylated on ROCKi treatment alone, which is even more striking in the EGFRi+ROCKi treatment. MYO1C is a key regulator of trafficking of cholesterol-enriched lipid rafts from intracellular storage compartments to the cell surface. Given that cholesterol is a critical component for autophagosome-lysosome fusion (49), it has been shown that loss of functional MYO1C led to an accumulation of autophagic structures, indicating a selective block in the autophagosome-lysosome fusion step and therefore, a defect in autophagic cargo degradation (50). The SNARE proteins play important roles in autophagy by mediating membrane fusion events that are required for the closure of isolation membranes into autophagosomes and the maturation of autophagosomes via fusion with endosomes or lysosomes for degradation (51, 52). Here, we found that when ROCK activity is inhibited two phosphosites of STX12 are downregulated, which is a SNARE protein that has been proposed to be required for autophagosome maturation in drosophila (53). Finally, ROCK inhibition also resulted in a very strong downregulation in the phosphorylation status of multiple sites of the actin-associated protein SYNPO2

that is involved in the autophagosome formation (54). Taken these data together seem to indicate a key role of these phosphorylation events in regulating proteins involved in autophagy, and their inhibition potentially leads to autophagy blockade.

Crosstalk of Autophagy and UPS—Interestingly, on inhibition of autophagy by ROCKi we observed a significant upregulation on the expression levels of core and regulatory subunits of the proteasome, implicating a potential activation of the ubiquitin-proteasome system (UPS) as a compensatory mechanism of cells to reduce the burden of accumulated autophagic substrates. A protein network of the detected multiple proteasomal subunit proteins (ANOVA significant) and their increased abundance levels in ROCKi- and EGFRi+ROCKi-treated cells compared with the DMSO and EGFRi treatments are illustrated in Fig. 7*A*. Among them, we detected proteins of the α- and β- subunits of the 20S core structure of the proteasome in the mammalian cells, including the catalytic proteasome β1 subunit, PSMB1. However, although our proteome data indicate a potential crosstalk between the two major degradation systems, complementary experiments to measure whether proteasomal activity is indeed enhanced on EGFRi+ROCKi treatment need to be performed to confirm our hypothesis.

DISCUSSION

Triple-negative breast cancer is an aggressive BC subtype, which suffers from the absence of known drug targets and is associated with an especially poor prognosis (55). Based on previous work (18), which revealed that the combination of EGFR and ROCK inhibitors effectively reduced TNBC cell growth by inducing cell cycle arrest, we here complement these previous findings by providing an insight into the molecular mechanisms triggered by the combinatorial EGFRi+ROCKi treatment.

Using a quantitative (phospho)proteomics approach to compare the proteome changes on single and combination treatments, we identify autophagy activation as a potential mechanism of the cells' response to treatment. We show that EGFR inhibition by gefitinib induces autophagy activation in TNBC cells, which was evident from the increased expression levels of several autophagy protein markers (*e.g.* MAP1LC3, GABARAP) and the formation of autophagic vacuoles. Moreover, we found that co-inhibition of EGFR and ROCK causes accumulation of autophagic vacuoles in triple-negative breast cancer cells and subsequent findings revealed that this accumulation is caused by the inhibition of autophagic flux as a result of ROCK activity inhibition. EGFR inhibition with tyrosine kinase inhibitors (TKIs) and neutralizing antibodies have been reported to upregulate autophagy in many cancer cells (56–58), including recent reports that suggest a role of endosomal-accumulated inactive EGFR in autophagy initiation on EGFR-TKI inhibition (59, 60). However, the specific function of this induction in cancer remains biphasic. In some studies, autophagy induction serves a cytoprotective response in cancer cells, whereas other studies report that enhanced autophagy after treatment with inhibitors can result in autophagic cell death (61). In this study, our results suggest that autophagy induction has a pro-survival role in triple-negative breast cancer cells on gefitinib treatment.

In addition to the contradicting literature regarding EGFR inhibitors and autophagy, ROCK activity has also been linked to this process, albeit with conflicting opinions regarding its function. Inhibition of ROCK activity can lead to autophagy impairment and cell death (62), whereas ROCK activity is required for starvation-mediated autophagy, because ROCK inhibition resulted in a decreased number of autophagosomes in cells under starvation conditions (63). Conversely, a study by Mleczak *et al*., showed that ROCK activity inhibited autophagy whereas the opposite was true for ROCK inhibition, which enhanced the autophagy response on starvation and led to the accumulation of enlarged early autophagosomes that matured into enlarged late degradative autolysosomes (64). Here, we show that ROCK activity is required for gefitinib-induced autophagy and that inhibition of ROCK leads to autophagy blockade and accumulation of autophagic vacuoles because of impaired autophagosome clearance. Given the key roles of the cytoskeleton in the different stages of autophagy, we speculate that the ROCKi-associated cytoskeletal changes are responsible for the blockage of autophagy. Indeed, our proteome data revealed major expression changes associated to the actin- and microtubule- cytoskeleton, which could cause a block during various steps of the autophagic pathway from the early stages of phagophore formation and expansion to vesicle trafficking and fusion with the lysosomes. In line with this reasoning, we found that the number of observed autophagic vacuoles in our EGFRi+ROCKi combination treatment in the TNBC cells was at a similar level as after the addition of CLQ, which blocks the fusion of autophagosomes and lysosomes, to EGFRi single treatment.

Interestingly, on ROCK inhibition, and subsequently autophagy impairment, we observed a significant upregulation of several proteasomal subunit proteins indicating a potential link between the autophagy and the ubiquitin-proteasome system, which is the other major intracellular pathway for protein degradation in mammalian cells. Indeed, in agreement with our findings, extensive evidence indicates that connections and crosstalk exist between the two systems, which are interconnected and inhibition of one system leads to a compensatory upregulation of the other system (65–67). However, although our proteome data indicates upregulation of the proteasome on autophagy inhibition, as discussed above, further experiments to assess the increased proteasomal activity *in vitro* are necessary to confirm the crosstalk.

In summary, our proteomic and functional data indicate that the activation of autophagy, on EGFR inhibition in triple-negative breast cancer cells, can be impaired by co-inhibition of ROCK activity, ultimately leading to TNBC cell death (Fig. 7*B*). We therefore believe that our data support the clinical potential

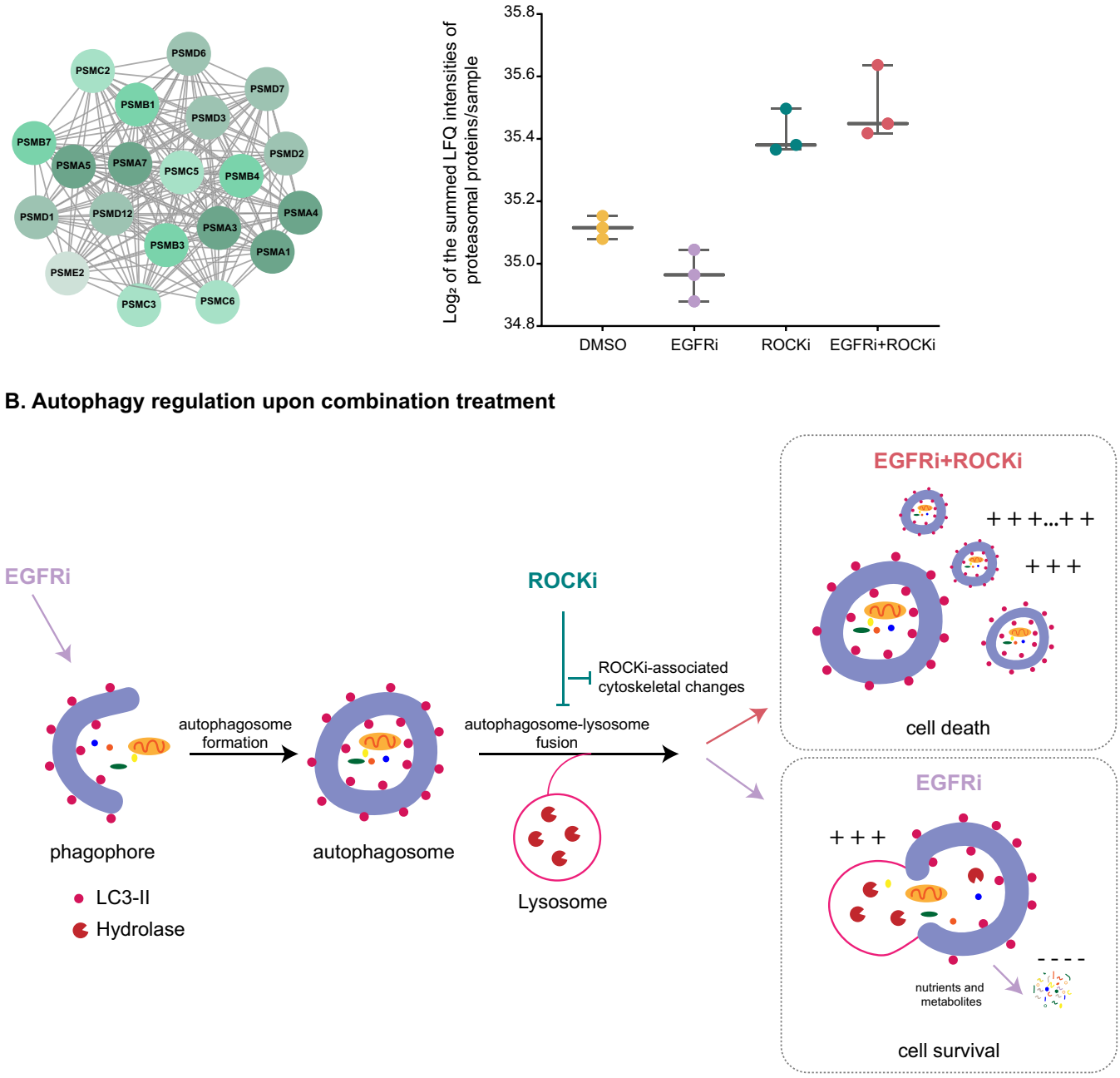

FIG. 7. **Regulation of proteasomal subunits and autophagy on EGFR and/or ROCK inhibition.** *A*, String network of all the differentially expressed (ANOVA significant) proteasomal subunit proteins and their relative abundance across the different treatments displayed by summing their LFQ intensities. *B*, EGFR inhibition induces autophagic flux in TNBC cells, which can be impaired on co-inhibition of ROCK activity leading to an increased accumulation of autophagic vacuoles and possibly autophagic cell death.

of therapeutically inhibiting autophagy for improved cancer therapy.

DATA AVAILABILITY

All mass spectrometry proteomics data have been deposited to the ProteomeXchange Consortium via the PRIDE partner repository with the dataset identifier PXD013821.

* This work was supported by the Netherlands Organization for Scientific Research (NWO) through a VIDI grant for M.A. (723.012.102) and Proteins@Work, a program of the National Roadmap Large-scale Research Facilities of the Netherlands (project number 184.032.201) and the Dutch Cancer Society (10304) for S.R., M.A. and D.S.P. The authors declare that they have no conflicts of interest with the contents of this article.

This article contains supplemental Figures and Table.

** To whom correspondence should be addressed: E-mail: m.altelaar@uu.nl.

Author contributions: S.R., S.I., and S.v.D. performed research; S.R. and M.A. analyzed data; S.R., D.S.P., and M.A. wrote the paper; D.S.P. and M.A. designed research.

REFERENCES

1. Wahba, H. A., and El-Hadaad, H. A. (2015) Current approaches in treatment of triple-negative breast cancer. *Cancer Biol. Med.* **12,** 106–16
2. Kalimutho, M., Parsons, K., Mittal, D., Lopez, J. A., Srihari, S., and Khanna, K. K. (2015) Targeted therapies for triple-negative breast cancer: combating a stubborn disease. *Trends Pharmacol. Sci.* **36,** 822–846
3. Crown, J., O'Shaughnessy, J., and Gullo, G. (2012) Emerging targeted therapies in triple-negative breast cancer. *Ann. Oncol*. **23,** vi56–vi65
4. Nakai, K., Hung, M. C., and Yamaguchi, H. (2016) A perspective on anti-EGFR therapies targeting triple-negative breast cancer. *Am. J. Cancer Res.* **6,** 1609–1623
5. Shen, M., Jiang, Y. Z., Wei, Y., Ell, B., Sheng, X., Esposito, M., Kang, J., Hang, X., Zheng, H., Rowicki, M., Zhang, L., Shih, W. J., Celia-Terrassa, T., Liu, Y., Cristea, I., Shao, Z. M., and Kang, Y. (2019) Tinagl1 suppresses triple-negative breast cancer progression and metastasis by simultaneously inhibiting integrin/FAK and EGFR signaling. *Cancer Cell* **35,** 64–80
6. Foidart, P., Yip, C., Radermacher, J., Blacher, S., Lienard, M., Montero-Ruiz, L., Maquoi, E., Montaudon, E., Chateau-Joubert, S., Collignon, J., Coibion, M., Jossa, V., Marangoni, E., Noel, A., Sounni, N. E., and Jerusalem, G. (2019) Expression of MT4-MMP, EGFR, and RB in triple-negative breast cancer strongly sensitizes tumors to erlotinib and palbociclib combination therapy. Clin. Cancer Res. **25,** 1838–1850
7. Kinsey, C. G., Camolotto, S. A., Boespflug, A. M., Guillen, K. P., Foth, M., Truong, A., Schuman, S. S., Shea, J. E., Seipp, M. T., Yap, J. T., Burrell, L. D., Lum, D. H., Whisenant, J. R., Gilcrease, G. W., Cavalieri, C. C., Rehbein, K. M., Cutler, S. L., Affolter, K. E., Welm, A. L., Welm, B. E., Scaife, C. L., Snyder, E. L., and McMahon, M. (2019) Protective autophagy elicited by RAF→MEK→ERK inhibition suggests a treatment strategy for RAS-driven cancers. *Nat. Med.* doi: 10.1038/s41591-019-0367-9
8. Bryant, K. L., Stalnecker, C. A., Zeitouni, D., Klomp, J. E., Peng, S., Tikunov, A. P., Gunda, V., Pierobon, M., Waters, A. M., George, S. D., Tomar, G., Papke, B., Hobbs, G. A., Yan, L., Hayes, T. K., Diehl, J. N., Goode, G. D., Chaika, N. V., Wang, Y., Zhang, G.-F., Witkiewicz, A. K., Knudsen, E. S., Petricoin, E. F., Singh, P. K., Macdonald, J. M., Tran, N. L., Lyssiotis, C. A., Ying, H., Kimmelman, A. C., Cox, A. D., and Der, C. J. (2019) Combination of ERK and autophagy inhibition as a treatment approach for pancreatic cancer. *Nat. Med.* doi: 10.1038/s41591-019-0368-8
9. Kroemer, G., Mariño, G., and Levine, B. (2010) Autophagy and the integrated stress response. Mol. Cell **40,** 280–293
10. Klionsky DJ and Emr SD. (2000) Autophagy as a regulated pathway of cellular degradation. *Science* **290,** 1717–1721
11. Feng, Y., He, D., Yao, Z., and Klionsky, D. J. (2013) The machinery of macroautophagy. *Cell Res.* **24,** 24
12. Kimmelman AC. (2011) The dynamic nature of autophagy in cancer. *Genes Dev.* **25,** 1999–2010
13. Degenhardt, K., Mathew, R., Beaudoin, B., Bray, K., Anderson, D., Chen, G., Mukherjee, C., Shi, Y., Gelinas, C., Fan, Y., Nelson, D. A., Jin, S., and White, E. (2006) Autophagy promotes tumor cell survival and restricts necrosis, inflammation, and tumorigenesis. *Cancer Cell* **10,** 51–64
14. Dragowska, W. H., Weppler, S. A., Wang, J. C., Wong, L. Y., Kapanen, A. I., Rawji, J. S., Warburton, C., Qadir, M. A., Donohue, E., Roberge, M., Gorski, S. M., Gelmon, K. A., and Bally, M. B. (2013) Induction of autophagy is an early response to gefitinib and a potential therapeutic target in breast cancer. *PLoS ONE* **8,** e76503
15. Paglin, S., Hollister, T., Delohery, T., Hackett, N., McMahill, M., Sphicas, E., Domingo, D., and Yahalom, J. (2001) A novel response of cancer cells to radiation involves autophagy and formation of acidic vesicles. *Cancer Res.* **61,** 439–444
16. Kanzawa, T., Germano, I. M., Komata, T., Ito, H., Kondo, Y., and Kondo, S. (2004) Role of autophagy in temozolomide-induced cytotoxicity for malignant glioma cells. *Cell Death Differ.* **11,** 448–457
17. Boya, P., Gonzalez-Polo, R. A., Casares, N., Perfettini, J. L., Dessen, P., Larochette, N., Metivier, D., Meley, D., Souquere, S., Yoshimori, T., Pierron, G., Codogno, P., and Kroemer, G. (2005) Inhibition of macroautophagy triggers apoptosis. *Mol. Cell. Biol.* **25,** 1025–1040
18. Iskit, S., Lieftink, C., Halonen, P., Shahrabi, A., Possik, P. A., Beijersbergen, R. L., and Peeper, D. S. (2016) Integrated in vivo genetic and pharmacologic screening identifies co-inhibition of EGRF and ROCK as a potential treatment regimen for triple-negative breast cancer. *Oncotarget* **7,** 42859–42872
19. Wang, Y., Yang, F., Gritsenko, M. A., Wang, Y., Clauss, T., Liu, T., Shen, Y., Monroe, M. E., Lopez-Ferrer, D., Reno, T., Moore, R. J., Klemke, R. L., Camp, D. G., 2nd, and Smith, R. D. (2011) Reversed-phase chromatography with multiple fraction concatenation strategy for proteome profiling of human MCF10A cells. *Proteomics* **11,** 2019–2026
20. Post, H., Penning, R., Fitzpatrick, M. A., Garrigues, L. B., Wu, W., MacGillavry, H. D., Hoogenraad, C. C., Heck, A. J., and Altelaar, A. F. (2017) Robust, sensitive, and automated phosphopeptide enrichment optimized for low sample amounts applied to primary hippocampal neurons. *J. Proteome Res.* **16,** 728–737
21. Cox J and Mann M. (2008) MaxQuant enables high peptide identification rates, individualized p.p.b.-range mass accuracies and proteome-wide protein quantification. *Nat. Biotechnol.* **26,** 1367–1372
22. Cox, J., Neuhauser, N., Michalski, A., Scheltema, R. A., Olsen, J. V., and Mann, M. (2011) Andromeda: a peptide search engine integrated into the MaxQuant environment. J. Proteome Res. **10,** 1794–1805
23. Cox, J., Hein, M. Y., Luber, C. A., Paron, I., Nagaraj, N., and Mann, M. (2014) Accurate proteome-wide label-free quantification by delayed normalization and maximal peptide ratio extraction, termed MaxLFQ. *Mol. Cell. Proteomics* **13,** 2513–2526
24. Tyanova, S., Temu, T., Sinitcyn, P., Carlson, A., Hein, M. Y., Geiger, T., Mann, M., and Cox, J. (2016) The Perseus computational platform for comprehensive analysis of (prote)omics data. *Nat. Methods* **13,** 731–740
25. Huang da W, Sherman BT and Lempicki RA. (2009) Systematic and integrative analysis of large gene lists using DAVID bioinformatics resources. *Nat. Protoc.* **4,** 44–57
26. Huang da W, Sherman BT and Lempicki RA. (2009) Bioinformatics enrichment tools: paths toward the comprehensive functional analysis of large gene lists. *Nucleic Acids Res.* **37,** 1–13
27. Doncheva, N. T., Morris, J. H., Gorodkin, J., and Jensen, L. J. (2019) Cytoscape StringApp: Network analysis and visualization of proteomics data. *J. Proteome Res.* **18,** 623–632
28. Shannon, P., Markiel, A., Ozier, O., Baliga, N. S., Wang, J. T., Ramage, D., Amin, N., Schwikowski, B., and Ideker, T. (2003) Cytoscape: a software environment for integrated models of biomolecular interaction networks. *Genome Res.* **13,** 2498–2504
29. Kang, J.-H., Jiang, Y., Toita, R., Oishi, J., Kawamura, K., Han, A., Mori, T., Niidome, T., Ishida, M., Tatematsu, K., Tanizawa, K., and Katayama, Y. (2007) Phosphorylation of Rho-associated kinase (Rho-kinase/ROCK/ROK) substrates by protein kinases A and C. *Biochimie* **89,** 39–47
30. Weidberg, H., Shvets, E., Shpilka, T., Shimron, F., Shinder, V., and Elazar, Z. (2010) LC3 and GATE-16/GABARAP subfamilies are both essential yet act differently in autophagosome biogenesis. *EMBO J.* **29,** 1792–1802
31. Krick, R., Busse, R. A., Scacioc, A., Stephan, M., Janshoff, A., Thumm, M., and Kuhnel, K. (2012) Structural and functional characterization of the two phosphoinositide binding sites of PROPPINs, a beta-propeller protein family. *Proc. Natl. Acad. Sci. U.S.A.* **109,** E2042–9
32. Ward, C., Martinez-Lopez, N., Otten, E. G., Carroll, B., Maetzel, D., Singh, R., Sarkar, S., and Korolchuk, V. I. (2016) Autophagy, lipophagy and lysosomal lipid storage disorders. *Biochim. Biophys. Acta* **1861,** 269–284
33. Kim, E., Goraksha-Hicks, P., Li, L., Neufeld, T. P., and Guan, K. L. (2008) Regulation of TORC1 by Rag GTPases in nutrient response. *Nat. Cell Biol.* **10,** 935–945
34. Xie, R., Nguyen, S., McKeehan, K., Wang, F., McKeehan, W. L., and Liu, L. (2011) Microtubule-associated protein 1S (MAP1S) bridges autophagic components with microtubules and mitochondria to affect autophagosomal biogenesis and degradation. *J. Biol. Chem.* **286,** 10367–10377
35. Klionsky, D. J., Abdalla, F. C., Abeliovich, H., Abraham, R. T., Acevedo-Arozena, A., Adeli, K., Agholme, L., Agnello, M., Agostinis, P., Aguirre-Ghiso, J. A., Ahn, H. J., Ait-Mohamed, O., Ait-Si-Ali, S., Akematsu, T., Akira, S., Al-Younes, H. M., Al-Zeer, M. A., Albert, M. L., Albin, R. L., Alegre-Abarrategui, J., Aleo, M. F., Alirezaei, M., Almasan, A., Almonte-Becerril, M., Amano, A., Amaravadi, R., Amarnath, S., Amer, A. O.,

Andrieu-Abadie, N., Anantharam, V., Ann, D. K., Anoopkumar-Dukie, S., Aoki, H., Apostolova, N., Arancia, G., Aris, J. P., Asanuma, K., Asare, N. Y., Ashida, H., Askanas, V., Askew, D. S., Auberger, P., Baba, M., Backues, S. K., Baehrecke, E. H., Bahr, B. A., Bai, X. Y., Bailly, Y., Baiocchi, R., Baldini, G., Balduini, W., Ballabio, A., Bamber, B. A., Bampton, E. T., Banhegyi, G., Bartholomew, C. R., Bassham, D. C., Bast, R. C., Jr, Batoko, H., Bay, B. H., Beau, I., Bechet, D. M., Begley, T. J., Behl, C., Behrends, C., Bekri, S., Bellaire, B., Bendall, L. J., Benetti, L., Berliocchi, L., Bernardi, H., Bernassola, F., Besteiro, S., Bhatia-Kissova, I., Bi, X., Biard-Piechaczyk, M., Blum, J. S., Boise, L. H., Bonaldo, P., Boone, D. L., Bornhauser, B. C., Bortoluci, K. R., Bossis, I., Bost, F., Bourquin, J. P., Boya, P., Boyer-Guittaut, M., Bozhkov, P. V., Brady, N. R., Brancolini, C., Brech, A., Brenman, J. E., Brennand, A., Bresnick, E. H., Brest, P., Bridges, D., Bristol, M. L., Brookes, P. S., Brown, E. J., Brumell, J. H., Brunetti-Pierri, N., Brunk, U. T., Bulman, D. E., Bultman, S. J., Bultynck, G., Burbulla, L. F., Bursch, W., Butchar, J. P., Buzgariu, W., Bydlowski, S. P., Cadwell, K., Cahova, M., Cai, D., Cai, J., Cai, Q., Calabretta, B., Calvo-Garrido, J., Camougrand, N., Campanella, M., Campos-Salinas, J., Candi, E., Cao, L., Caplan, A. B., Carding, S. R., Cardoso, S. M., Carew, J. S., Carlin, C. R., Carmignac, V., Carneiro, L. A., Carra, S., Caruso, R. A., Casari, G., Casas, C., Castino, R., Cebollero, E., Cecconi, F., Celli, J., Chaachouay, H., Chae, H. J., Chai, C. Y., Chan, D. C., Chan, E. Y., Chang, R. C., Che, C. M., Chen, C. C., Chen, G. C., Chen, G. Q., Chen, M., Chen, Q., Chen, S. S., Chen, W., Chen, X., Chen, X., Chen, X., Chen, Y. G., Chen, Y., Chen, Y., Chen, Y. J., Chen, Z., Cheng, A., Cheng, C. H., Cheng, Y., Cheong, H., Cheong, J. H., Cherry, S., Chess-Williams, R., Cheung, Z. H., Chevet, E., Chiang, H. L., Chiarelli, R., Chiba, T., Chin, L. S., Chiou, S. H., Chisari, F. V., Cho, C. H., Cho, D. H., Choi, A. M., Choi, D., Choi, K. S., Choi, M. E., Chouaib, S., Choubey, D., Choubey, V., Chu, C. T., Chuang, T. H., Chueh, S. H., Chun, T., Chwae, Y. J., Chye, M. L., Ciarcia, R., Ciriolo, M. R., Clague, M. J., Clark, R. S., Clarke, P. G., Clarke, R., Codogno, P., Coller, H. A., Colombo, M. I., Comincini, S., Condello, M., Condorelli, F., Cookson, M. R., Coombs, G. H., Coppens, I., Corbalan, R., Cossart, P., Costelli, P., Costes, S., Coto-Montes, A., Couve, E., Coxon, F. P., Cregg, J. M., Crespo, J. L., Cronje, M. J., Cuervo, A. M., Cullen, J. J., Czaja, M. J., D'Amelio, M., Darfeuille-Michaud, A., Davids, L. M., Davies, F. E., De Felici, M., de Groot, J. F., de Haan, C. A., De Martino, L., De Milito, A., De Tata, V., Debnath, J., Degterev, A., Dehay, B., Delbridge, L. M., Demarchi, F., Deng, Y. Z., Dengjel, J., Dent, P., Denton, D., Deretic, V., Desai, S. D., Devenish, R. J., Di Gioacchino, M., Di Paolo, G., Di Pietro, C., Diaz-Araya, G., Diaz-Laviada, I., Diaz-Meco, M. T., Diaz-Nido, J., Dikic, I., Dinesh-Kumar, S. P., Ding, W. X., Distelhorst, C. W., Diwan, A., Djavaheri-Mergny, M., Dokudovskaya, S., Dong, Z., Dorsey, F. C., Dosenko, V., Dowling, J. J., Doxsey, S., Dreux, M., Drew, M. E., Duan, Q., Duchosal, M. A., Duff, K., Dugail, I., Durbeej, M., Duszenko, M., Edelstein, C. L., Edinger, A. L., Egea, G., Eichinger, L., Eissa, N. T., Ekmekcioglu, S., El-Deiry, W. S., Elazar, Z., Elgendy, M., Ellerby, L. M., Eng, K. E., Engelbrecht, A. M., Engelender, S., Erenpreisa, J., Escalante, R., Esclatine, A., Eskelinen, E. L., Espert, L., Espina, V., Fan, H., Fan, J., Fan, Q. W., Fan, Z., Fang, S., Fang, Y., Fanto, M., Fanzani, A., Farkas, T., Farre, J. C., Faure, M., Fechheimer, M., Feng, C. G., Feng, J., Feng, Q., Feng, Y., Fesus, L., Feuer, R., Figueiredo-Pereira, M. E., Fimia, G. M., Fingar, D. C., Finkbeiner, S., Finkel, T., Finley, K. D., Fiorito, F., Fisher, E. A., Fisher, P. B., Flajolet, M., Florez-McClure, M. L., Florio, S., Fon, E. A., Fornai, F., Fortunato, F., Fotedar, R., Fowler, D. H., Fox, H. S., Franco, R., Frankel, L. B., Fransen, M., Fuentes, J. M., Fueyo, J., Fujii, J., Fujisaki, K., Fujita, E., Fukuda, M., Furukawa, R. H., Gaestel, M., Gailly, P., Gajewska, M., Galliot, B., Galy, V., Ganesh, S., Ganetzky, B., Ganley, I. G., Gao, F. B., Gao, G. F., Gao, J., Garcia, L., Garcia-Manero, G., Garcia-Marcos, M., Garmyn, M., Gartel, A. L., Gatti, E., Gautel, M., Gawriluk, T. R., Gegg, M. E., Geng, J., Germain, M., Gestwicki, J. E., Gewirtz, D. A., Ghavami, S., Ghosh, P., Giammarioli, A. M., Giatromanolaki, A. N., Gibson, S. B., Gilkerson, R. W., Ginger, M. L., Ginsberg, H. N., Golab, J., Goligorsky, M. S., Golstein, P., Gomez-Manzano, C., Goncu, E., Gongora, C., Gonzalez, C. D., Gonzalez, R., Gonzalez-Estevez, C., Gonzalez-Polo, R. A., Gonzalez-Rey, E., Gorbunov, N. V., Gorski, S., Goruppi, S., Gottlieb, R. A., Gozuacik, D., Granato, G. E., Grant, G. D., Green, K. N., Gregorc, A., Gros, F., Grose, C., Grunt, T. W., Gual, P., Guan, J. L., Guan, K. L., Guichard, S. M., Gukovskaya, A. S., Gukovsky, I., Gunst, J., Gustafsson, A. B., Halayko, A. J., Hale, A. N., Halonen, S. K., Hamasaki, M., Han, F., Han, T., Hancock, M. K., Hansen, M., Harada, H., Harada, M., Hardt, S. E., Harper, J. W., Harris, A. L., Harris, J., Harris, S. D., Hashimoto, M., Haspel, J. A., Hayashi, S., Hazelhurst, L. A., He, C., He, Y. W., Hebert, M. J., Heidenreich, K. A., Helfrich, M. H., Helgason, G. V., Henske, E. P., Herman, B., Herman, P. K., Hetz, C., Hilfiker, S., Hill, J. A., Hocking, L. J., Hofman, P., Hofmann, T. G., Hohfeld, J., Holyoake, T. L., Hong, M. H., Hood, D. A., Hotamisligil, G. S., Houwerzijl, E. J., Hoyer-Hansen, M., Hu, B., Hu, C. A., Hu, H. M., Hua, Y., Huang, C., Huang, J., Huang, S., Huang, W. P., Huber, T. B., Huh, W. K., Hung, T. H., Hupp, T. R., Hur, G. M., Hurley, J. B., Hussain, S. N., Hussey, P. J., Hwang, J. J., Hwang, S., Ichihara, A., Ilkhanizadeh, S., Inoki, K., Into, T., Iovane, V., Iovanna, J. L., Ip, N. Y., Isaka, Y., Ishida, H., Isidoro, C., Isobe, K., Iwasaki, A., Izquierdo, M., Izumi, Y., Jaakkola, P. M., Jaattela, M., Jackson, G. R., Jackson, W. T., Janji, B., Jendrach, M., Jeon, J. H., Jeung, E. B., Jiang, H., Jiang, H., Jiang, J. X., Jiang, M., Jiang, Q., Jiang, X., Jiang, X., Jimenez, A., Jin, M., Jin, S., Joe, C. O., Johansen, T., Johnson, D. E., Johnson, G. V., Jones, N. L., Joseph, B., Joseph, S. K., Joubert, A. M., Juhasz, G., Juillerat-Jeanneret, L., Jung, C. H., Jung, Y. K., Kaarniranta, K., Kaasik, A., Kabuta, T., Kadowaki, M., Kagedal, K., Kamada, Y., Kaminskyy, V. O., Kampinga, H. H., Kanamori, H., Kang, C., Kang, K. B., Kang, K. I., Kang, R., Kang, Y. A., Kanki, T., Kanneganti, T. D., Kanno, H., Kanthasamy, A. G., Kanthasamy, A., Karantza, V., Kaushal, G. P., Kaushik, S., Kawazoe, Y., Ke, P. Y., Kehrl, J. H., Kelekar, A., Kerkhoff, C., Kessel, D. H., Khalil, H., Kiel, J. A., Kiger, A. A., Kihara, A., Kim, D. R., Kim, D. H., Kim, D. H., Kim, E. K., Kim, H. R., Kim, J. S., Kim, J. H., Kim, J. C., Kim, J. K., Kim, P. K., Kim, S. W., Kim, Y. S., Kim, Y., Kimchi, A., Kimmelman, A. C., King, J. S., Kinsella, T. J., Kirkin, V., Kirshenbaum, L. A., Kitamoto, K., Kitazato, K., Klein, L., Klimecki, W. T., Klucken, J., Knecht, E., Ko, B. C., Koch, J. C., Koga, H., Koh, J. Y., Koh, Y. H., Koike, M., Komatsu, M., Kominami, E., Kong, H. J., Kong, W. J., Korolchuk, V. I., Kotake, Y., Koukourakis, M. I., Kouri Flores, J. B., Kovacs, A. L., Kraft, C., Krainc, D., Kramer, H., Kretz-Remy, C., Krichevsky, A. M., Kroemer, G., Kruger, R., Krut, O., Ktistakis, N. T., Kuan, C. Y., Kucharczyk, R., Kumar, A., Kumar, R., Kumar, S., Kundu, M., Kung, H. J., Kurz, T., Kwon, H. J., La Spada, A. R., Lafont, F., Lamark, T., Landry, J., Lane, J. D., Lapaquette, P., Laporte, J. F., Laszlo, L., Lavandero, S., Lavoie, J. N., Layfield, R., Lazo, P. A., Le, W., Le Cam, L., Ledbetter, D. J., Lee, A. J., Lee, B. W., Lee, G. M., Lee, J., Lee, J. H., Lee, M., Lee, M. S., Lee, S. H., Leeuwenburgh, C., Legembre, P., Legouis, R., Lehmann, M., Lei, H. Y., Lei, Q. Y., Leib, D. A., Leiro, J., Lemasters, J. J., Lemoine, A., Lesniak, M. S., Lev, D., Levenson, V. V., Levine, B., Levy, E., Li, F., Li, J. L., Li, L., Li, S., Li, W., Li, X. J., Li, Y. B., Li, Y. P., Liang, C., Liang, Q., Liao, Y. F., Liberski, P. P., Lieberman, A., Lim, H. J., Lim, K. L., Lim, K., Lin, C. F., Lin, F. C., Lin, J., Lin, J. D., Lin, K., Lin, W. W., Lin, W. C., Lin, Y. L., Linden, R., Lingor, P., Lippincott-Schwartz, J., Lisanti, M. P., Liton, P. B., Liu, B., Liu, C. F., Liu, K., Liu, L., Liu, Q. A., Liu, W., Liu, Y. C., Liu, Y., Lockshin, R. A., Lok, C. N., Lonial, S., Loos, B., Lopez-Berestein, G., Lopez-Otin, C., Lossi, L., Lotze, M. T., Low, P., Lu, B., Lu, B., Lu, B., Lu, Z., Luciano, F., Lukacs, N. W., Lund, A. H., Lynch-Day, M. A., Ma, Y., Macian, F., MacKeigan, J. P., Macleod, K. F., Madeo, F., Maiuri, L., Maiuri, M. C., Malagoli, D., Malicdan, M. C., Malorni, W., Man, N., Mandelkow, E. M., Manon, S., Manov, I., Mao, K., Mao, X., Mao, Z., Marambaud, P., Marazziti, D., Marcel, Y. L., Marchbank, K., Marchetti, P., Marciniak, S. J., Marcondes, M., Mardi, M., Marfe, G., Marino, G., Markaki, M., Marten, M. R., Martin, S. J., Martinand-Mari, C., Martinet, W., Martinez-Vicente, M., Masini, M., Matarrese, P., Matsuo, S., Matteoni, R., Mayer, A., Mazure, N. M., McConkey, D. J., McConnell, M. J., McDermott, C., McDonald, C., McInerney, G. M., McKenna, S. L., McLaughlin, B., McLean, P. J., McMaster, C. R., McQuibban, G. A., Meijer, A. J., Meisler, M. H., Melendez, A., Melia, T. J., Melino, G., Mena, M. A., Menendez, J. A., Menna-Barreto, R. F., Menon, M. B., Menzies, F. M., Mercer, C. A., Merighi, A., Merry, D. E., Meschini, S., Meyer, C. G., Meyer, T. F., Miao, C. Y., Miao, J. Y., Michels, P. A., Michiels, C., Mijaljica, D., Milojkovic, A., Minucci, S., Miracco, C., Miranti, C. K., Mitroulis, I., Miyazawa, K., Mizushima, N., Mograbi, B., Mohseni, S., Molero, X., Mollereau, B., Mollinedo, F., Momoi, T., Monastyrska, I., Monick, M. M., Monteiro, M. J., Moore, M. N., Mora, R., Moreau, K., Moreira, P. I., Moriyasu, Y., Moscat, J., Mostowy, S., Mottram, J. C., Motyl, T., Moussa, C. E., Muller, S., Muller, S., Munger, K., Munz, C., Murphy, L. O., Murphy, M. E., Musaro, A., Mysorekar, I., Nagata, E., Nagata, K., Nahimana, A., Nair, U., Nakagawa, T., Nakahira, K., Nakano, H., Nakatogawa, H., Nanjundan, M., Naqvi, N. I., Narendra, D. P., Narita,

M., Navarro, M., Nawrocki, S. T., Nazarko, T. Y., Nemchenko, A., Netea, M. G., Neufeld, T. P., Ney, P. A., Nezis, I. P., Nguyen, H. P., Nie, D., Nishino, I., Nislow, C., Nixon, R. A., Noda, T., Noegel, A. A., Nogalska, A., Noguchi, S., Notterpek, L., Novak, I., Nozaki, T., Nukina, N., Nurnberger, T., Nyfeler, B., Obara, K., Oberley, T. D., Oddo, S., Ogawa, M., Ohashi, T., Okamoto, K., Oleinick, N. L., Oliver, F. J., Olsen, L. J., Olsson, S., Opota, O., Osborne, T. F., Ostrander, G. K., Otsu, K., Ou, J. H., Ouimet, M., Overholtzer, M., Ozpolat, B., Paganetti, P., Pagnini, U., Pallet, N., Palmer, G. E., Palumbo, C., Pan, T., Panaretakis, T., Pandey, U. B., Papackova, Z., Papassideri, I., Paris, I., Park, J., Park, O. K., Parys, J. B., Parzych, K. R., Patschan, S., Patterson, C., Pattingre, S., Pawelek, J. M., Peng, J., Perlmutter, D. H., Perrotta, I., Perry, G., Pervaiz, S., Peter, M., Peters, G. J., Petersen, M., Petrovski, G., Phang, J. M., Piacentini, M., Pierre, P., Pierrefite-Carle, V., Pierron, G., Pinkas-Kramarski, R., Piras, A., Piri, N., Platanias, L. C., Poggeler, S., Poirot, M., Poletti, A., Pous, C., Pozuelo-Rubio, M., Praetorius-Ibba, M., Prasad, A., Prescott, M., Priault, M., Produit-Zengaffinen, N., Progulske-Fox, A., Proikas-Cezanne, T., Przedborski, S., Przyklenk, K., Puertollano, R., Puyal, J., Qian, S. B., Qin, L., Qin, Z. H., Quaggin, S. E., Raben, N., Rabinowich, H., Rabkin, S. W., Rahman, I., Rami, A., Ramm, G., Randall, G., Randow, F., Rao, V. A., Rathmell, J. C., Ravikumar, B., Ray, S. K., Reed, B. H., Reed, J. C., Reggiori, F., Regnier-Vigouroux, A., Reichert, A. S., Reiners, J. J., Jr, Reiter, R. J., Ren, J., Revuelta, J. L., Rhodes, C. J., Ritis, K., Rizzo, E., Robbins, J., Roberge, M., Roca, H., Roccheri, M. C., Rocchi, S., Rodemann, H. P., Rodriguez de Cordoba, S., Rohrer, B., Roninson, I. B., Rosen, K., Rost-Roszkowska, M. M., Rouis, M., Rouschop, K. M., Rovetta, F., Rubin, B. P., Rubinsztein, D. C., Ruckdeschel, K., EBRucker 3rd, Rudich, A., Rudolf, E., Ruiz-Opazo, N., Russo, R., Rusten, T. E., Ryan, K. M., Ryter, S. W., Sabatini, D. M., Sadoshima, J., Saha, T., Saitoh, T., Sakagami, H., Sakai, Y., Salekdeh, G. H., Salomoni, P., Salvaterra, P. M., Salvesen, G., Salvioli, R., Sanchez, A. M., Sanchez-Alcazar, J. A., Sanchez-Prieto, R., Sandri, M., Sankar, U., Sansanwal, P., Santambrogio, L., Saran, S., Sarkar, S., Sarwal, M., Sasakawa, C., Sasnauskiene, A., Sass, M., Sato, K., Sato, M., Schapira, A. H., Scharl, M., Schatzl, H. M., Scheper, W., Schiaffino, S., Schneider, C., Schneider, M. E., Schneider-Stock, R., Schoenlein, P. V., Schorderet, D. F., Schuller, C., Schwartz, G. K., Scorrano, L., Sealy, L., Seglen, P. O., Segura-Aguilar, J., Seiliez, I., Seleverstov, O., Sell, C., Seo, J. B., Separovic, D., Setaluri, V., Setoguchi, T., Settembre, C., Shacka, J. J., Shanmugam, M., Shapiro, I. M., Shaulian, E., Shaw, R. J., Shelhamer, J. H., Shen, H. M., Shen, W. C., Sheng, Z. H., Shi, Y., Shibuya, K., Shidoji, Y., Shieh, J. J., Shih, C. M., Shimada, Y., Shimizu, S., Shintani, T., Shirihai, O. S., Shore, G. C., Sibirny, A. A., Sidhu, S. B., Sikorska, B., Silva-Zacarin, E. C., Simmons, A., Simon, A. K., Simon, H. U., Simone, C., Simonsen, A., Sinclair, D. A., Singh, R., Sinha, D., Sinicrope, F. A., Sirko, A., Siu, P. M., Sivridis, E., Skop, V., Skulachev, V. P., Slack, R. S., Smaili, S. S., Smith, D. R., Soengas, M. S., Soldati, T., Song, X., Sood, A. K., Soong, T. W., Sotgia, F., Spector, S. A., Spies, C. D., Springer, W., Srinivasula, S. M., Stefanis, L., Steffan, J. S., Stendel, R., Stenmark, H., Stephanou, A., Stern, S. T., Sternberg, C., Stork, B., Stralfors, P., Subauste, C. S., Sui, X., Sulzer, D., Sun, J., Sun, S. Y., Sun, Z. J., Sung, J. J., Suzuki, K., Suzuki, T., Swanson, M. S., Swanton, C., Sweeney, S. T., Sy, L. K., Szabadkai, G., Tabas, I., Taegtmeyer, H., Tafani, M., Takacs-Vellai, K., Takano, Y., Takegawa, K., Takemura, G., Takeshita, F., Talbot, N. J., Tan, K. S., Tanaka, K., Tanaka, K., Tang, D., Tang, D., Tanida, I., Tannous, B. A., Tavernarakis, N., Taylor, G. S., Taylor, G. A., Taylor, J. P., Terada, L. S., Terman, A., Tettamanti, G., Thevissen, K., Thompson, C. B., Thorburn, A., Thumm, M., Tian, F., Tian, Y., Tocchini-Valentini, G., Tolkovsky, A. M., Tomino, Y., Tonges, L., Tooze, S. A., Tournier, C., Tower, J., Towns, R., Trajkovic, V., Travassos, L. H., Tsai, T. F., Tschan, M. P., Tsubata, T., Tsung, A., Turk, B., Turner, L. S., Tyagi, S. C., Uchiyama, Y., Ueno, T., Umekawa, M., Umemiya-Shirafuji, R., Unni, V. K., Vaccaro, M. I., Valente, E. M., Van den Berghe, G., van der Klei, I. J., van Doorn, W., van Dyk, L. F., van Egmond, M., van Grunsven, L. A., Vandenabeele, P., Vandenberghe, W. P., Vanhorebeek, I., Vaquero, E. C., Velasco, G., Vellai, T., Vicencio, J. M., Vierstra, R. D., Vila, M., Vindis, C., Viola, G., Viscomi, M. T., Voitsekhovskaja, O. V., von Haefen, C., Votruba, M., Wada, K., Wade-Martins, R., Walker, C. L., Walsh, C. M., Walter, J., Wan, X. B., Wang, A., Wang, C., Wang, D., Wang, F., Wang, F., Wang, G., Wang, H., Wang, H. G., Wang, H. D., Wang, J., Wang, K., Wang, M., Wang, R. C., Wang, X., Wang, X., Wang, Y. J., Wang, Y., Wang, Z., Wang, Z. C., Wang, Z., Wansink, D. G., Ward, D. M., Watada, H., Waters, S. L., Webster, P., Wei, L., Weihl, C. C., Weiss, W. A., Welford, S. M., Wen, L. P., Whitehouse, C. A., Whitton, J. L., Whitworth, A. J., Wileman, T., Wiley, J. W., Wilkinson, S., Willbold, D., Williams, R. L., Williamson, P. R., Wouters, B. G., Wu, C., Wu, D. C., Wu, W. K., Wyttenbach, A., Xavier, R. J., Xi, Z., Xia, P., Xiao, G., Xie, Z., Xie, Z., Xu, D. Z., Xu, J., Xu, L., Xu, X., Yamamoto, A., Yamamoto, A., Yamashina, S., Yamashita, M., Yan, X., Yanagida, M., Yang, D. S., Yang, E., Yang, J. M., Yang, S. Y., Yang, W., Yang, W. Y., Yang, Z., Yao, M. C., Yao, T. P., Yeganeh, B., Yen, W. L., Yin, J. J., Yin, X. M., Yoo, O. J., Yoon, G., Yoon, S. Y., Yorimitsu, T., Yoshikawa, Y., Yoshimori, T., Yoshimoto, K., You, H. J., Youle, R. J., Younes, A., Yu, L., Yu, L., Yu, S. W., Yu, W. H., Yuan, Z. M., Yue, Z., Yun, C. H., Yuzaki, M., Zabirnyk, O., Silva-Zacarin, E., Zacks, D., Zacksenhaus, E., Zaffaroni, N., Zakeri, Z., HJZeh 3rd, Zeitlin, S. O., Zhang, H., Zhang, H. L., Zhang, J., Zhang, J. P., Zhang, L., Zhang, L., Zhang, M. Y., Zhang, X. D., Zhao, M., Zhao, Y. F., Zhao, Y., Zhao, Z. J., Zheng, X., Zhivotovsky, B., Zhong, Q., Zhou, C. Z., Zhu, C., Zhu, W. G., Zhu, X. F., Zhu, X., Zhu, Y., Zoladek, T., Zong, W. X., Zorzano, A., Zschocke, J., and Zuckerbraun, B. (2012) Guidelines for the use and interpretation of assays for monitoring autophagy. *Autophagy* **8,** 445–544

36. Roux, P. P., Shahbazian, D., Vu, H., Holz, M. K., Cohen, M. S., Taunton, J., Sonenberg, N., and Blenis, J. (2007) RAS/ERK signaling promotes site-specific ribosomal protein S6 phosphorylation via RSK and stimulates cap-dependent translation. *J. Biol. Chem.* **282,** 14056–14064
37. Chen, B., Zhang, W., Gao, J., Chen, H., Jiang, L., Liu, D., Cao, Y., Zhao, S., Qiu, Z., Zeng, J., Zhang, S., and Li, W. (2014) Downregulation of ribosomal protein S6 inhibits the growth of non-small cell lung cancer by inducing cell cycle arrest, rather than apoptosis. *Cancer Lett.* **354,** 378–389
38. Guo, S., Liang, Y., Murphy, S. F., Huang, A., Shen, H., Kelly, D. F., Sobrado, P., and Sheng, Z. (2015) A rapid and high content assay that measures cyto-ID-stained autophagic compartments and estimates autophagy flux with potential clinical applications. *Autophagy* **11,** 560–572
39. Mauthe, M., Orhon, I., Rocchi, C., Zhou, X., Luhr, M., Hijlkema, K. J., Coppes, R. P., Engedal, N., Mari, M., and Reggiori, F. (2018) Chloroquine inhibits autophagic flux by decreasing autophagosome-lysosome fusion. *Autophagy* **14,** 1435–1455
40. Amano, M., Nakayama, M., and Kaibuchi, K. (2010) Rho-kinase/ROCK: A key regulator of the cytoskeleton and cell polarity. *Cytoskeleton* **67,** 545–554
41. Kast DJ and Dominguez R. (2017) The cytoskeleton-autophagy connection. *Curr. Biol*. **27,** R318–R326
42. Kruppa, A. J., Kendrick-Jones, J., and Buss, F. (2016) Myosins, actin and autophagy. *Traffic* **17,** 878–890
43. Kast, D. J., Zajac, A. L., Holzbaur, E. L., Ostap, E. M., and Dominguez, R. (2015) WHAMM directs the Arp2/3 complex to the ER for autophagosome biogenesis through an actin comet tail mechanism. *Curr. Biol.* **25,** 1791–1797
44. Holland, P., and Simonsen, A. (2015) Actin shapes the autophagosome. *Nat. Cell Biol.* **17,** 1094–1096
45. Mi, N., Chen, Y., Wang, S., Chen, M., Zhao, M., Yang, G., Ma, M., Su, Q., Luo, S., Shi, J., Xu, J., Guo, Q., Gao, N., Sun, Y., Chen, Z., and Yu, L. (2015) CapZ regulates autophagosomal membrane shaping by promoting actin assembly inside the isolation membrane. *Nat. Cell Biol.* **17,** 1112–1123
46. Mackeh, R., Perdiz, D., Lorin, S., Codogno, P., and Pous, C. (2013) Autophagy and microtubules - new story, old players. *J. Cell Sci.* **126,** 1071–1080
47. Fass, E., Shvets, E., Degani, I., Hirschberg, K., and Elazar, Z. (2006) Microtubules support production of starvation-induced autophagosomes but not their targeting and fusion with lysosomes. *J. Biol. Chem.* **281,** 36303–36316
48. Illenberger, S., Drewes, G., Trinczek, B., Biernat, J., Meyer, H. E., Olmsted, J. B., Mandelkow, E. M., and Mandelkow, E. (1996) Phosphorylation of microtubule-associated proteins MAP2 and MAP4 by the protein kinase p110mark. Phosphorylation sites and regulation of microtubule dynamics. *J. Biol. Chem.* **271,** 10834–10843
49. Fraldi, A., Annunziata, F., Lombardi, A., Kaiser, H. J., Medina, D. L., Spampanato, C., Fedele, A. O., Polishchuk, R., Sorrentino, N. C., Simons, K., and Ballabio, A. (2010) Lysosomal fusion and SNARE function are impaired by cholesterol accumulation in lysosomal storage disorders. *EMBO J.* **29,** 3607–3620
50. Brandstaetter, H., Kishi-Itakura, C., Tumbarello, D. A., Manstein, D. J., and Buss, F. (2014) Loss of functional MYO1C/myosin 1c, a motor protein

involved in lipid raft trafficking, disrupts autophagosome-lysosome fusion. *Autophagy* **10,** 2310–2323
51. Nair, U., Jotwani, A., Geng, J., Gammoh, N., Richerson, D., Yen, W.-L., Griffith, J., Nag, S., Wang, K., Moss, T., Baba, M., McNew James, A., Jiang, X., Reggiori, F., Melia Thomas, J., and Klionsky Daniel, J. (2011) SNARE proteins are required for macroautophagy. *Cell* **146,** 290–302
52. Wang, Y., Li, L., Hou, C., Lai, Y., Long, J., Liu, J., Zhong, Q., and Diao, J. (2016) SNARE-mediated membrane fusion in autophagy. *Sem. Cell Develop. Biol*. **60,** 97–104
53. Lu, Y., Zhang, Z., Sun, D., Sweeney Sean, T., and Gao, F.-B. (2013) Syntaxin 13, a genetic modifier of mutant CHMP2B in frontotemporal dementia, is required for autophagosome maturation. *Mol. Cell* **52,** 264–271
54. Ulbricht, A., Eppler Felix, J., Tapia Victor, E., van der Ven Peter, F. M., Hampe, N., Hersch, N., Vakeel, P., Stadel, D., Haas, A., Saftig, P., Behrends, C., Fürst Dieter, O., Volkmer, R., Hoffmann, B., Kolanus W and J Höhfeld. (2013) Cellular mechanotransduction relies on tension-induced and chaperone-assisted autophagy. *Curr. Biol.* **23,** 430–435
55. Tan, D. S., Marchio, C., Jones, R. L., Savage, K., Smith, I. E., Dowsett, M., and Reis-Filho, J. S. (2008) Triple negative breast cancer: molecular profiling and prognostic impact in adjuvant anthracycline-treated patients. *Breast Cancer Res. Treat.* **111,** 27–44
56. Jutten, B., and Rouschop, K. M. (2014) EGFR signaling and autophagy dependence for growth, survival, and therapy resistance. *Cell Cycle* **13,** 42–51
57. Li, X., and Fan, Z. (2010) The epidermal growth factor receptor antibody cetuximab induces autophagy in cancer cells by downregulating HIF-1alpha and Bcl-2 and activating the beclin 1/hVps34 complex. *Cancer Res.* **70,** 5942–5952
58. Wei, Y., Zou, Z., Becker, N., Anderson, M., Sumpter, R., Xiao, G., Kinch, L., Koduru, P., Christudass, C. S., Veltri, R. W., Grishin, N. V., Peyton, M., Minna, J., Bhagat, G., and Levine, B. (2013) EGFR-mediated Beclin 1 phosphorylation in autophagy suppression, tumor progression, and tumor chemoresistance. *Cell* **154,** 1269–1284
59. Tan, X., Thapa, N., Sun, Y., and Anderson, R. A. (2015) A kinase-independent role for EGF receptor in autophagy initiation. *Cell* **160,** 145–160
60. Tan, X., Lambert, P. F., Rapraeger, A. C., and Anderson, R. A. (2016) Stress-induced EGFR trafficking: mechanisms, functions, and therapeutic implications. *Trends Cell Biol*. **26,** 352–366
61. Cui, J., Hu, Y. F., Feng, X. M., Tian, T., Guo, Y. H., Ma, J. W., Nan, K. J., and Zhang, H. Y. (2014) EGFR inhibitors and autophagy in cancer treatment. *Tumour Biol.* **35,** 11701–11709
62. Gurkar, A. U., Chu, K., Raj, L., Bouley, R., Lee, S. H., Kim, Y. B., Dunn, S. E., Mandinova, A., and Lee, S. W. (2013) Identification of ROCK1 kinase as a critical regulator of Beclin1-mediated autophagy during metabolic stress. *Nat. Commun.* **4,** 2189
63. Aguilera, M. O., Beron, W., and Colombo, M. I. (2012) The actin cytoskeleton participates in the early events of autophagosome formation on starvation induced autophagy. *Autophagy* **8,** 1590–1603
64. Mleczak, A., Millar, S., Tooze, S. A., Olson, M. F., and Chan, E. Y. (2013) Regulation of autophagosome formation by Rho kinase. *Cell Signal.* **25,** 1–11
65. Wang, X. J., Yu, J., Wong, S. H., Cheng, A. S., Chan, F. K., Ng, S. S., Cho, C. H., Sung, J. J., and Wu, W. K. (2013) A novel crosstalk between two major protein degradation systems: regulation of proteasomal activity by autophagy. *Autophagy* **9,** 1500–1508
66. Korolchuk, V. I., Menzies, F. M., and Rubinsztein, D. C. (2010) Mechanisms of cross-talk between the ubiquitin-proteasome and autophagy-lysosome systems. *FEBS Lett.* **584,** 1393–1398
67. Cha-Molstad, H., Yu, J. E., Feng, Z., Lee, S. H., Kim, J. G., Yang, P., Han, B., Sung, K. W., Yoo, Y. D., Hwang, J., McGuire, T., Shim, S. M., Song, H. D., Ganipisetti, S., Wang, N., Jang, J. M., Lee, M. J., Kim, S. J., Lee, K. H., Hong, J. T., Ciechanover, A., Mook-Jung, I., Kim, K. P., Xie, X.-Q., Kwon, Y. T., and Kim, B. Y. (2017) p62/SQSTM1/Sequestosome-1 is an N-recognin of the N-end rule pathway which modulates autophagosome biogenesis. Nature Commun. **8,** 102
68. Kaimal, V., Bardes, E. E., Tabar, S. C., Jegga, A. G., and Aronow, B. J. (2010) ToppCluster: a multiple gene list feature analyzer for comparative enrichment clustering and network-based dissection of biological systems. *Nucleic Acids Res*. **38,** W96–W102